



HAL
open science

What Controls the Skill of General Circulation Models to Simulate the Seasonal Cycle in Water Isotopic Composition in the Tibetan Plateau Region?

Xiaoyi Shi, Camille Risi, Laurent Li, Xuejie Wang, Tao Pu, Guotao Zhang,
Yuan Zhang, Zhiyuan Wang, Yanlong Kong

► **To cite this version:**

Xiaoyi Shi, Camille Risi, Laurent Li, Xuejie Wang, Tao Pu, et al.. What Controls the Skill of General Circulation Models to Simulate the Seasonal Cycle in Water Isotopic Composition in the Tibetan Plateau Region?. *Journal of Geophysical Research: Atmospheres*, 2022, 127 (22), pp.106551. 10.1029/2022jd037048 . hal-03893447

HAL Id: hal-03893447

<https://hal.science/hal-03893447>

Submitted on 11 Dec 2022

HAL is a multi-disciplinary open access archive for the deposit and dissemination of scientific research documents, whether they are published or not. The documents may come from teaching and research institutions in France or abroad, or from public or private research centers.

L'archive ouverte pluridisciplinaire **HAL**, est destinée au dépôt et à la diffusion de documents scientifiques de niveau recherche, publiés ou non, émanant des établissements d'enseignement et de recherche français ou étrangers, des laboratoires publics ou privés.

Key Points:

- Models systematically underestimate the precipitation isotopic seasonality both in the southern and northern TP
- The inter-model spread of precipitation isotopic seasonality in the southern TP is driven by the spread of upstream precipitation
- The westerlies dominate the inter-model spread of precipitation isotopic seasonality in the northern TP

Supporting Information:

Supporting Information may be found in the online version of this article.

Correspondence to:

Z. Wang and Y. Kong,
wzhy@zjnu.edu.cn;
ylkong@mail.iggcas.ac.cn









Citation:

Shi, X., Risi, C., Li, L., Wang, X., Pu, T., Zhang, G., et al. (2022). What controls the skill of general circulation models to simulate the seasonal cycle in water isotopic composition in the Tibetan Plateau region? *Journal of Geophysical Research: Atmospheres*, 127, e2022JD037048. <https://doi.org/10.1029/2022JD037048>

Received 1 MAY 2022

Accepted 9 NOV 2022

What Controls the Skill of General Circulation Models to Simulate the Seasonal Cycle in Water Isotopic Composition in the Tibetan Plateau Region?

Xiaoyi Shi^{1,2,3} , Camille Risi⁴ , Laurent Li⁴ , Xuejie Wang⁵, Tao Pu^{3,6} , Guotao Zhang⁷ , Yuan Zhang^{4,8} , Zhiyuan Wang¹ , and Yanlong Kong⁹ 

¹College of Geography and Environment Sciences, Zhejiang Normal University, Jinhua, China, ²Laboratoire de Météorologie Dynamique, IPSL, Sorbonne Université, Paris, France, ³National Field Science Observation and Research Station of Yulong Snow Mountain Cryosphere and Sustainable Development, Northwest Institute of Eco-Environment and Resources, Chinese Academy of Sciences, Lanzhou, China, ⁴Laboratoire de Météorologie Dynamique, IPSL, CNRS, Sorbonne Université, Paris, France, ⁵Institute of International Rivers and Eco-security, Yunnan University, Kunming, China, ⁶State Key Laboratory of Cryospheric Sciences, Northwest Institute of Eco-environment and Resources, Chinese Academy of Sciences, Lanzhou, China, ⁷Key Laboratory of Land Surface Pattern and Simulation, Institute of Geographic Sciences and Natural Resources Research, Chinese Academy of Sciences, Beijing, China, ⁸Laboratoire des Sciences du Climat et de l'Environnement (LSCE), IPSL, CEA/CNRS/UVSQ, Gif sur Yvette, France, ⁹Institute of Geology and Geophysics, Chinese Academy of Sciences, Beijing, China

Abstract This study evaluates the simulation of the seasonal cycle of water isotopic composition over Tibetan Plateau regions (TP) from six isotope-enabled general circulation models (GCMs) participating in the second Phase of Stable Water Isotope Intercomparison Group. For both meteorological factors (precipitation rate and wind field) and isotopic composition, GCMs generally agree with reanalysis data and in-situ observations, but there is a significant spread across models and the isotopic seasonality is systematically underestimated. In the southern TP, the precipitation isotopic composition is more depleted in summer than in winter, and the amplitude of the simulated isotopic seasonal variations is primarily driven by the amplitude of the simulated upstream precipitation. In contrast, in the northern TP, the precipitation isotopic composition is more depleted in winter than in summer, and the amplitude of the simulated seasonal variability of isotopes is mainly driven by the simulated strength of the zonal wind. We conclude that the skill of a GCM to simulate the seasonal cycle in the isotopic composition depends mainly on the skill of the GCM to simulate the Indian summer monsoon precipitation and the westerlies. The same causes contributing to the underestimated seasonality at present-day may also contribute to the underestimated $\delta^{18}\text{O}$ change at the mid-Holocene.

Plain Language Summary The stable isotopic composition of water is determined by the relative abundances of heavier to lighter isotopologues. Isotope-enabled general circulation models (GCMs) simulate water isotope composition considering several physical processes operating in the hydrologic cycle. Therefore, a comparison between observed and simulated values provides a better understanding of the processes constraining the isotope values. However, the simulated water isotopic composition is sensitive to various physical processes and parameterization schemes. In this study, we investigate how the model biases in the representation of atmospheric processes affect the simulation of isotopic composition over the Tibetan Plateau (TP). We compare the simulated isotopic composition in precipitation and water vapor to in-situ and satellite measurements. Our analysis indicates that most GCMs underestimate the seasonality of the isotopic composition in the precipitation and vapor. In the southern TP, the spread of upstream precipitation is an important factor controlling the inter-model spread in isotopic seasonality. In the northern TP, the westerlies majorly control isotope biases.

1. Introduction

The Tibetan Plateau and its surroundings contain the largest number of glaciers outside the polar Regions (Yao et al., 2012). Natural archives (e.g., ice core records) of past precipitation isotopic compositions can be used to infer information about past climate change. The isotopic signals recorded in the ice cores and authigenic carbonates can be used to reconstruct paleoclimate (Thompson et al., 2000; B. Yang et al., 2007; Yao et al., 1996; Yao, Shi, & Thompson, 1997; Yao, Thompson, et al., 1997; Yu, Tian, et al., 2016; Zhao et al., 2017), and paleoelevations

(Bershaw et al., 2012; Botsyun et al., 2019; Hren et al., 2009; Shen & Poulsen, 2019). It also reflects the evolution of atmospheric circulation (Gao et al., 2016; Joswiak et al., 2013; Kaspari et al., 2007; X. Yang et al., 2012; X. X. Yang et al., 2018; Yu, Yao, et al., 2016). However, the interpretation of isotopic signals remains challenging due to the numerous and complex processes involved in the hydrologic cycle, such as changes in moisture sources, recycling, and transport processes (e.g., An et al., 2017; Cai & Tian, 2020; Hren et al., 2009; Kong et al., 2019; Kurita & Yamada, 2008; Midhun et al., 2018; Sengupta & Sarkar, 2006; Shi et al., 2020; Tian et al., 2007, 2008; Wu et al., 2015, 2019; Yu et al., 2008, 2014). Over the TP, the isotopic variation of precipitation reflects the integrated information of the interaction between the westerlies and monsoon, in conjunction with the local recycling. Therefore, TP offers exceptional access to understanding the multiple processes affecting the present-day and past precipitation isotopic composition.

To improve our knowledge of mechanisms controlling the water stable isotope variations, isotope-enabled GCMs are now frequently used (Dee et al., 2018; Lee et al., 2012; Risi et al., 2010; Werner et al., 2011; Yoshimura et al., 2008). GCMs simulate the three-dimensional circulation in the global atmosphere with a horizontal resolution of the order of 100 km. Physical processes that act on a smaller scale, such as convection and clouds, are parameterized. In isotope-enabled GCMs, water isotopologues are implemented as passive tracers that undergo exactly the same processes as standard water and fractionate during phase changes. Such isotope-enabled GCMs have also been widely used to better understand how isotopes preserve the past climatic signal at paleoclimatic time scales (Bühler et al., 2020; Feng et al., 2013; Hu et al., 2019; Liu et al., 2014; Risi et al., 2010; Tabor et al., 2018; Yu et al., 2020) and at the inter-annual to decadal time scales (Hu et al., 2019; Ishizaki et al., 2012; Münch & Laepple, 2018; Vuille et al., 2003; Vuille & Werner, 2004). For instance, the stable oxygen isotopic ratio in ice cores is widely used as a proxy for temperature because of the significant positive correlation between air temperature and precipitation $\delta^{18}\text{O}$ (An et al., 2016; Yao et al., 1996, 2013).

The water isotopic composition is sensitive to the simulated meteorological variables and to the representation of physical processes governing convection and cloud (Bony et al., 2008; Field et al., 2014; Hu et al., 2018; Schmidt et al., 2005). Convection and cloud parameterizations, which rely on many simplifications or assumptions (Del Genio, 2012; Rio et al., 2019), are responsible for a significant part of model biases in simulating present-day or past climate and for the large inter-model spread in climate change projections (Randall et al., 2013; Stevens & Bony, 2013; Webb et al., 2015). Thus, parameterization in the model may also contribute to model biases and inter-model spread in simulating isotopic composition aside from other model biases (Midhun & Ramesh, 2016; Nimya et al., 2022).

The goal of this study is to assess the skill of GCMs to simulate the seasonal distribution of the water isotopic composition over the TP, and to analyze how bias in the simulation of meteorological variables translates into corresponding rain isotope biases. With this aim, we compare eight simulations from six GCMs that participated in SWING2. In Section 2 we describe the SWING2 simulations and observations. In Section 3 we evaluate the simulated meteorological variables and isotopic composition with respect to observations. Biases and inter-model spread are estimated and interpreted in Section 4. In Section 5 paleoclimate implications of these results are discussed.

2. Models and Observations

2.1. SWING2 Simulations

We use eight simulations from six GCMs (CAM2, MIROC32, HadAM3, isoGSM, LMDZ, HadCM3) that were archived by SWING2 (Risi et al., 2012a). As shown in Table 1, it is worth noting that all simulations are a few generations older than the current generation model when we use them to do relative work. All models are forced by observed sea surface temperatures, except HadCM3, which is an ocean-atmosphere coupled simulation. Since HadCM3 and HadAM3 have the same atmospheric physical properties but differ by their sea surface temperatures, this is an opportunity to test the relative importance of the physical representation of atmospheric processes and boundary conditions. Of the eight simulations, two were nudged by reanalysis winds (Table 1) to ensure a more realistic simulation of the large-scale circulation (Risi et al., 2010; Yoshimura et al., 2008). The other simulations are “free running” corresponding to standard Atmospheric Model Intercomparison Program-style simulations (Gates, 1992) forced by observed sea surface temperatures. The analysis is based on the multi-year-mean monthly-mean isotope data and meteorological variables from 1980 to 2001, covering the common period across

Table 1
Information on Isotope-Enabled GCMs in This Study

Models	Horizontal resolution	Vertical resolution	Nudging	Whole period	References
CAM2	2.81° × 2.81°	26	Free	1959–2003	Lee et al. (2007)
MIROC32	2.84° × 2.80°	20	Free	1979–2007	Kurita et al. (2011)
IsoGSM	1.875° × 1.875°	17	Free or nudged (u, v, T) by NCEP	1979–2009	Yoshimura et al. (2008)
LMDZ	3.75° × 2.5°	19	free or nudged (u,v) by ECMWF	1979–2007	Risi et al. (2010)
HadAM3	3.75° × 2.5°	17	Free	1870–2001	Sime et al. (2009)
HadCM3	3.75° × 2.5°	17	Free	-	Tindall et al. (2009)

all the archived model simulations. The multi-year analysis is justified by the fact that seasonal variations are larger than year-to-year variations, both in observations (Figure S2 of Supporting Information S1 vs. Figure 2c) and in all simulations (Figure S1 of Supporting Information S1 vs. Figure 2f) over most of the Tibetan Plateau. We checked using a two-tailed student *t*-test that at Lhasa and Delingha, seasonal variation can be robustly extracted from inter-annual variation with a confidence level larger than 95% in all models and in observations from GNIP/TNIP (except for HadCM3 and GNIP/TNIP at Lhasa and isoGSM free at Delingha where the confidence level is 90%) (Table S3 and Table S4 of Supporting Information S2). This is consistent with previous studies on the TP (e.g., Shi et al., 2020), although the results may be different in India (Midhun & Ramesh, 2016; Nimya et al., 2022). As a further check, we tried to plot all our figures using all available years for each simulation (Table 1) and half of the available years from 1991 to 2001, instead of using a common period (1980–2001) for the multi-year-mean monthly-mean. We find that the results are very similar (Figure S3–S14 of Supporting Information S1). Therefore, our results are robust with respect to inter-annual variation. All model outputs were resampled into a 3.75° × 2.5° grid in longitude-latitude, in order to facilitate the inter-comparison.

2.2. Observational Data Sets

To assess the performance of models, monthly precipitation-weighted $\delta^{18}\text{O}$ ($\delta^{18}\text{O}_p$) from 0° N to 60° N and 60° E to 140° E in the Global Network for Isotopes in Precipitation (GNIP) and the Tibetan Plateau Network for Isotopes in Precipitation (TNIP) database are used. In total, we use $\delta^{18}\text{O}$ data at 169 stations. We use the entire period available online for each station, as detailed in Table S1 of Supporting Information S2.

The observations of precipitation composition are spatially discrete and represent only the days when precipitation falls. To assess the spatial distribution of the isotopic composition with better spatio-temporal coverage, we also use the observed water vapor δD (δD_v) retrievals from Tropical Emission Spectrometer (TES, Worden et al. [2006, 2007]). To first order, δD variations mirror those of $\delta^{18}\text{O}$ but are 8 times larger (Dansgaard, 1964). In addition, observations and model simulations suggest that isotopic variations at different altitudes in the troposphere vary in concert (e.g., Bony et al., 2008; He et al., 2015; Shi et al., 2020). This is physically justified by the fact that deep convection efficiently mixes the vapor in the vertical as demonstrated by cloud-resolving model simulations (Risi et al., 2021). The water vapor δD from TES significantly correlates with the observed $\delta^{18}\text{O}$ in precipitation from GNIP ($r = 0.6$, $p < 0.05$). Therefore, water vapor δD variations at 500 hPa are expected to be relevant for the interpretation of $\delta^{18}\text{O}_p$ variations at the surface (e.g., Shi et al., 2020). We consider the period 2004–2007 when the sampling frequency is maximum for TES.

We use the retrievals at 500 hPa, which is close to the maximal retrieval sensitivity, and select only profiles with valid quality flags and degrees of freedom of the signal greater than 0.5. Furthermore, TES retrieves isotopic profiles only under clear sky conditions. This induces a bias. Ideally, co-locating the daily outputs with TES retrievals, that is, sampled at the same location and on the same days as the TES measurements would be necessary to mitigate this bias. Moreover, we should consider the effect of instrument sensitivity by convolving the outputs with observed averaging kernels for each day and location. This operation slightly reduces the amplitude of δD_v variations by a few ‰ (Risi et al., 2012a; Shi et al., 2020). Unfortunately, daily outputs are not available from SWING2 simulations. Therefore, we cannot co-locate the daily output of the model with the satellite observations and cannot convolve them with an appreciable averaging kernel. Using daily outputs in a particular model, He et al. (2015) estimated this bias in Lhasa. At the global scale, Risi et al. (2012a) estimated this bias to

be about 5‰. Therefore, we will focus on δD variations that are larger than 5‰. In addition, all types of isotopic variations are smoothed in the TES observations (e.g., Risi et al., 2012a, 2013b). This is because, during the retrieval process, the algorithm starts with an initial isotope profile, called *a-priori* profile, which is horizontally and temporally uniform. Since the sensitivity of the instrument is not perfect, at each altitude, the final retrieved δD_v will be a combination of this *a-priori* profile and the real δD_v values at different altitudes. For example, the TES retrievals for different seasons are biased toward the *a-priori* profile, and therefore seasonal variations are underestimated. When interpreting the results, we will thus keep in mind that if the simulations were perfectly realistic, they would show larger variations than observed. More details on TES measurements, retrieval methods, and uncertainties can be found in earlier studies (Risi et al., 2013; Worden et al., 2006, 2007).

For observed water isotopologues in precipitation, inter-annual variations are generally smaller than seasonal variations (Figure S2, Table S3, and Table S4 of Supporting Information S2; Shi et al. [2020]). So, the seasonal variations that we analyze with the GNIP/TNIP or TES datasets are robust and informative even though the time periods are different from the simulations (Shi et al., 2020). The multi-year-mean monthly-mean wind vectors near the surface from January 1948 to December 2020 are employed to investigate the climate mean state, which is acquired from the NCEP-NCAR reanalysis with a spatial resolution of $2.5^\circ \times 2.5^\circ$ (Kalnay et al., 1996). We also tried a higher-resolution ERA5 reanalysis and found very similar results (Figure S16 of Supporting Information S1). Precipitation data from the Global Precipitation Climatology Project (GPCP) with a resolution of $0.5^\circ \times 0.5^\circ$ (Adler et al., 2018) are used in our study (January 1979–December 2020). For a higher-resolution comparison, we also used the India Meteorological Department's (IMD) high-resolution gridded rainfall dataset ($0.25^\circ \times 0.25^\circ$; Pai et al. [2015]). All observations were bi-linearly interpolated to a $3.75^\circ \times 2.5^\circ$ grid (longitude \times latitude) for comparison with simulations.

2.3. Evaluation of the Simulated Meteorological Variables and Isotopic Composition

2.3.1. Precipitation and Large-Scale Circulation

The purpose of this section is to assess the skill of the simulations by comparing the multi-year average seasonal cycles of observed and simulated precipitation rates and wind fields. The spatial patterns of precipitation rates and wind fields during December-January-February (DJF) and June-July-August (JJA) over the TP and adjacent regions are shown in Figure 1, for both observations and multi-model mean. We warn that the multi-model mean can mix different spatial patterns of the individual models, but this is a first step before investigating the individual models in more detail in the next sub-sections. The spatio-temporal variability of summer precipitation over the TP is complex and is mainly controlled by a combination of monsoon dynamics and regional moisture recycling (Chen et al., 2012; Mölg et al., 2014; Yang & Yao, 2020). It can be found that the models can capture the spatial patterns of the simulated multi-model average precipitation rates and wind fields (Figures 1d–1f) compared to those observed by GPCP and NCEP-NCAR (Figure 1 a-c) to a large extent.

The highest observed precipitation rate in JJA can be found in the central Himalayas, the west coast of India and the Western Ghats, the Bay of Bengal, and surrounding areas, in relation to the Indian summer monsoon (Kumar et al., 2014; Zhang et al., 2011). During the summer monsoon, the vapor is transported from the Bay of Bengal via a moisture corridor along the Brahmaputra River (Breitenbach et al., 2010; Chen et al., 2012; G. Wu & Zhang, 1998; K. Yang et al., 2014) (Figures 1a and 1d). In the multi-model mean, the model simulates relatively well the precipitation and circulation patterns. However, the SWING2 model overestimates the precipitation in the Southern part of India and the surrounding ocean (Figures 1a, 1c and 1g), except over a narrow band along the Western coast (as seen when compared with the high-resolution IMD dataset (Figure S25 of Supporting Information S1)). The overestimate of precipitation over most of Southern India is consistent with previous studies comparing GCMs with observations of the Indian monsoon precipitation (Gusain et al., 2020; Sperber et al., 2013). The underestimate of precipitation over the Western coast is consistent with Nimya et al. (2022).

In DJF, the observed precipitation is reduced compared to JJA (Figures 1b and 1e). In the northern part of west China, precipitation is mainly brought by mid-latitude westerlies (Tian et al., 2007). In the multi-model mean, the simulations are in good agreement with the observed distribution of precipitation and circulation patterns. It has been a long-lasting problem in the atmospheric modeling community that GCMs overestimate the precipitation rates over mountains and their foothills (e.g., Cordor & Sadourny, 2002; Jia et al., 2019; Su et al., 2013; Zhu & Yang, 2020). As a consequence, it is also a problem for the isotope modeling community

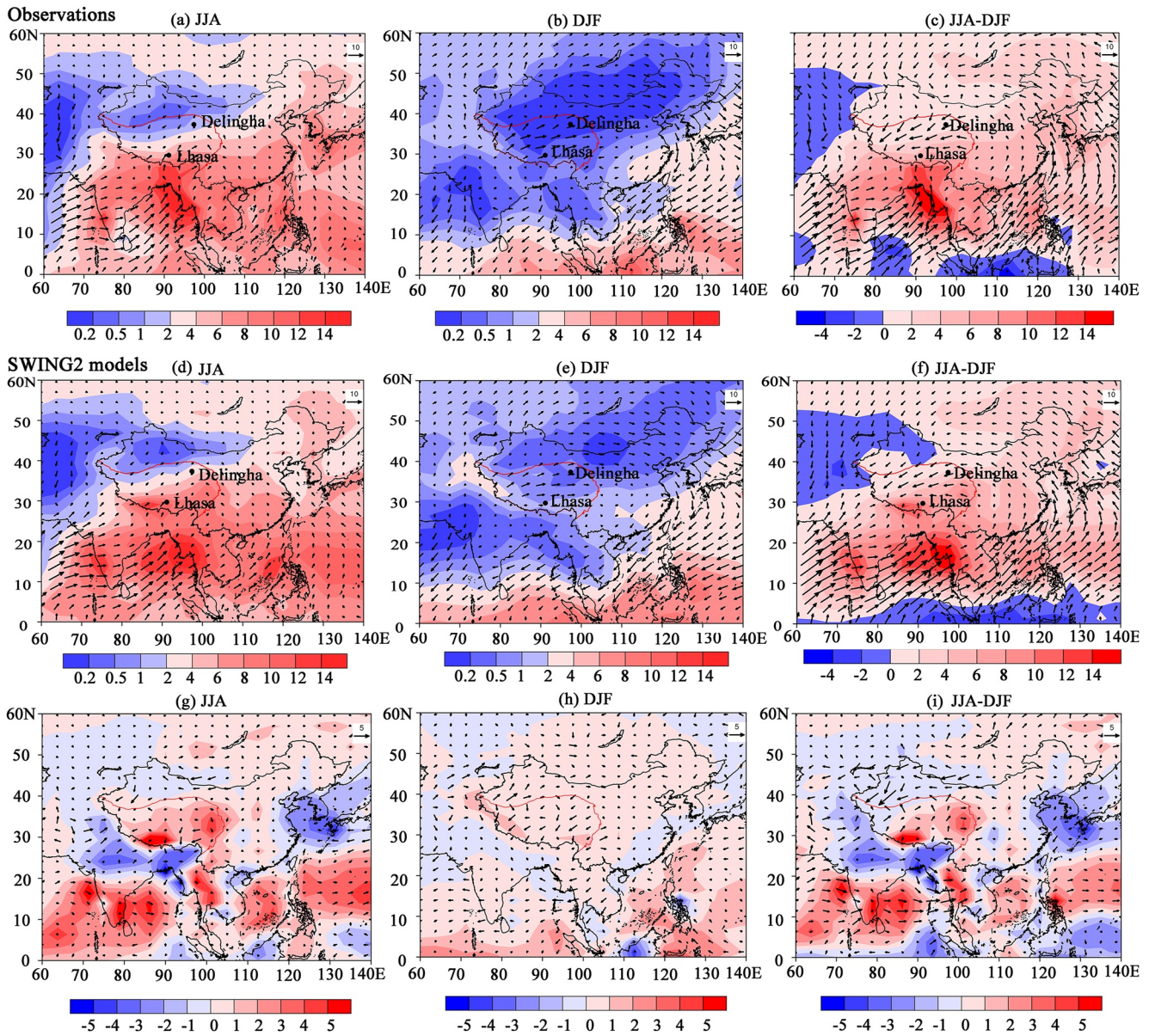


Figure 1. Precipitation rate (shaded, mm/d) from Global Precipitation Climatology Project (GPCP) and wind field (vector, m/s) near the surface from NCEP-NCAR reanalysis for JJA (a), DJF (b) and JJA-minus-DJF (c). (d)–(f) Same as panels a–c, but for models shown as multi-model mean. For each model m from 1 to M and each grid cell (i, j) , the multi-model mean of the variable \bar{X} , \bar{X} is computed by the following equation: $\bar{X}(i, j) = \sum_{m=1}^M X_m(i, j)/M$. For each model, the annual mean is calculated by averaging all months of all years at each location. The JJA and DJF averages are calculated by averaging all JJA and DJF months, respectively, of all years. Difference between simulated and observed precipitation rate (shaded) and near-surface winds (vectors) for JJA (g), DJF (h), and JJA-DJF (i). Observed precipitation comes from GPCP during the 1979–2020 period and observed winds come from NECP-NCAR during the 1948–2020. On each map, the location of Lhasa and Delingha, which will be investigated in more detail as representative stations for the Southern and Northern regions respectively, is indicated. The red contour shows the boundary of the Tibetan Plateau (higher than 3,000 m).

when trying to use these atmospheric models for mountainous regions, including over TP (Che et al., 2016; Gao et al., 2013; He et al., 2015). This may be due to the excessively diffusive properties of advection schemes (Codron & Sadourny, 2002; Yu et al., 2015).

The JJA-minus-DJF difference in observed precipitation rate shows positive values over most of South and East Asia (Figure 1c), which is emblematic of the monsoon climate of the region. The spatial pattern mainly reflects that of JJA precipitation rate. The zonal wind JJA-minus-DJF difference is positive over India and negative over the TP (Figure 1i), reflecting the enhanced monsoonal winds in summer and the dominant westerlies in

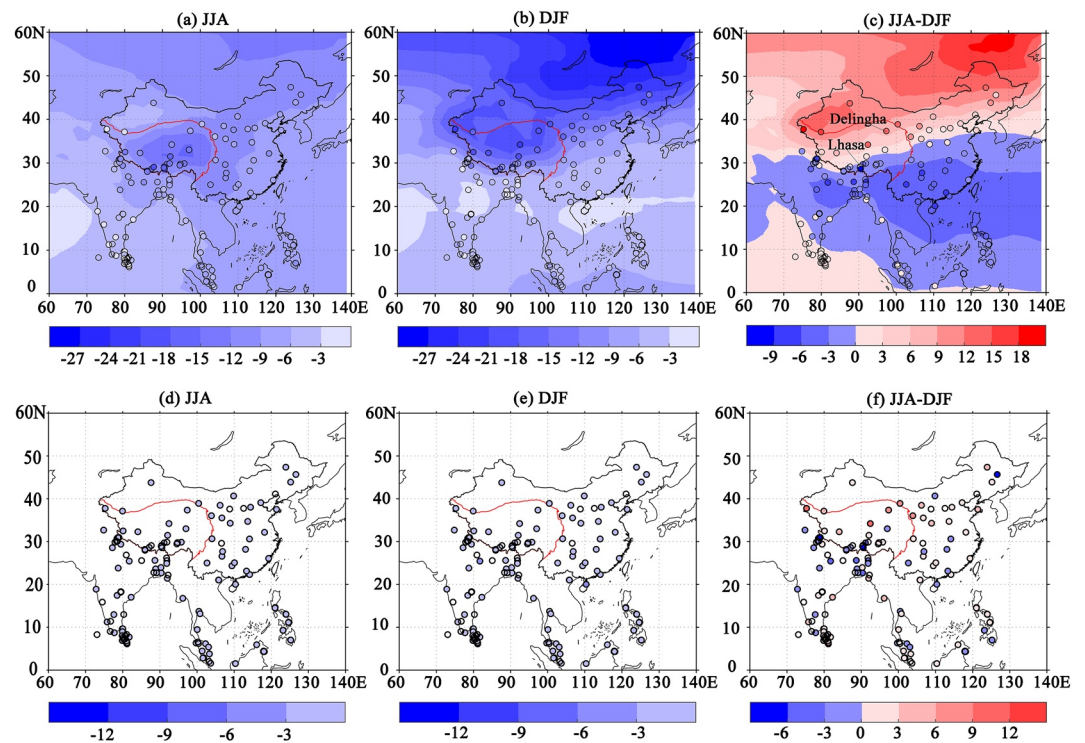


Figure 2. Precipitation $\delta^{18}\text{O}$ (‰) for JJA (a), DJF (b), and JJA-minus-DJF (c). Shaded patterns represent multi-model mean and colored circles represent the observation from Global Precipitation Climatology Project/Tibetan Plateau Network for Isotopes in Precipitation. Colored circles and shaded areas in upper panels keep the same color scale for a better visual inspection of differences between observations and simulations. (d)–(f) Difference between simulated and observed precipitation $\delta^{18}\text{O}$ for JJA (d), DJF, (e) and JJA-DJF (f).

winter. The multi-model mean agrees qualitatively well with the observed pattern (Figure 1f). However, the same model-data mismatches as for JJA, already mentioned earlier, arise.

2.4. Isotopic Composition

To evaluate the isotopic simulations, we use the GNIP and TNIP data. The observed $\delta^{18}\text{O}_p$ shows a minimum over the TP in both seasons (Figures 2a–2c), as expected from the altitude effect (Yao et al., 2013), and a poleward decrease in $\delta^{18}\text{O}_p$ in winter in northern China, as expected from the temperature and continental effects (Araguás-Araguás et al., 1998; Rozanski et al., 1993). These features are well reproduced qualitatively by the SWING2 models (Figures 2a–2c), as already shown by Zhang et al. (2011). However, the SWING2 models underestimate the observed depletion over the southern TP in summer. This underestimated depletion had already been noticed in previous studies and can be attributable to the coarse resolution of the topography or the underestimation of water vapor depletion by the Indian Monsoon (Shi et al., 2020; Yao et al., 2013).

For the $\delta^{18}\text{O}_p$ seasonality (JJA-minus-DJF) (Figure 2c), two distinct regions can be found, with positive values in the northern region (approximately north of 30°N) and negative values in the southern region (approximately south of 30°N). Hereafter, Lhasa and Delingha have more extended isotope datasets overlapping with all studied models for significantly long periods. Figure 2c shows that they are situated south and north of TP and nearly represent the zones of opposite water isotope seasonality. Therefore, these two stations are considered further for detailed study. Our definition of the two regions echoes previous studies. For example, Yao et al. (2013) divided the TP into three domains: the monsoon domain, the westerly domain, and the transition between these two domains (Araguás-Araguás et al., 1998). Note that although Lhasa is near the latitude where the sign of the JJA-DJF change, the depletion from the spring season to the monsoon season is robust across models (Section 3.4).

The seasonality of multi-model mean $\delta^{18}\text{O}_p$ can capture positive values in the northern region and negative values in the southern region (Figure 2c). The region with negative values extends further North than the observed

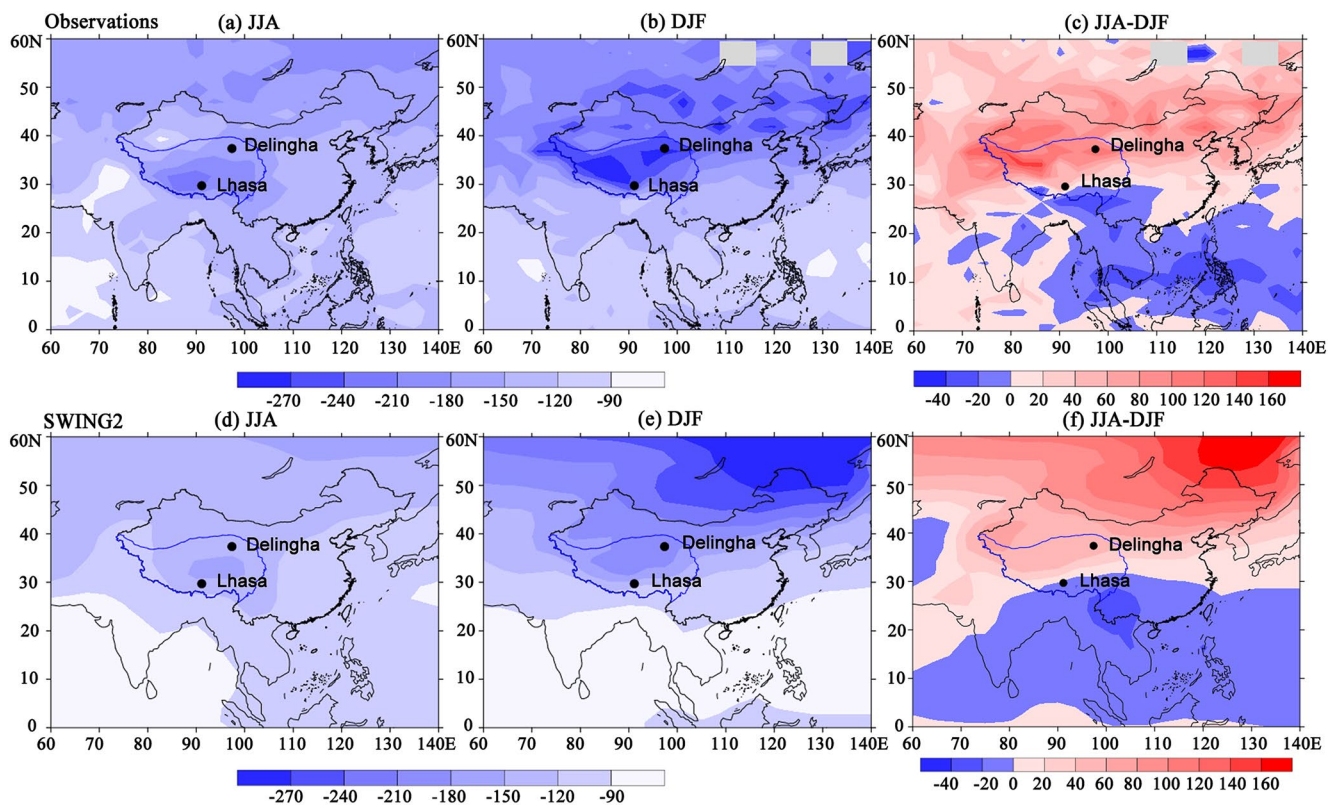


Figure 3. Mean water vapor δD (‰) at 500 hPa observed by Tibetan Plateau Network for Isotopes in Precipitation (TES) and simulated by multi-model mean from Stable Water Isotope Intercomparison Group 2 (SWING2) in JJA (a), (d), DJF (b), (e) and for JJA-minus-DJF (c), (f). The data period of 2004–2007 for TES and of 1980–2001 for SWING2 was used.

values, although there is some spread across models to this extent. As for precipitation, the biases in the seasonality of $\delta^{18}O_p$ (Figure 2f) mainly reflect the biases of $\delta^{18}O_p$ during the monsoon period (Figure 2d).

Figure 3 looks similar to Figure 2 but for δD_v . The spatial distribution of δD_v simulated by multi-model mean and observed by TES is similar to that of $\delta^{18}O_p$ in JJA, DJF, and seasonality. This is consistent with the fact that the isotopic composition in precipitation varies in concert with water vapor (Shi et al., 2020).

2.5. Inter-Model Spread

As discussed above, models on average exhibit some biases relative to the observations. But the models also show significant differences between each other. The goal of this section is to quantify these inter-model differences. Figure 4 shows maps of inter-model standard deviation of the seasonality (JJA-minus-DJF) in precipitation, zonal wind, $\delta^{18}O_p$ and δD_v near the surface.

For precipitation rate seasonality, the SWING2 models show maximum spread over Bangladesh, Bhutan, western India, and the southern TP (Figure 4a). This corresponds to the region where the simulated precipitation rate seasonality is high, and also where the multi-model mean differs the most compared to observations (Figure 1i). In particular, over the southern TP where the multi-model mean overestimates the precipitation, the inter-model standard deviation is of a similar magnitude as the multi-model mean. This suggests that some models produce realistic precipitation while others strongly overestimate it. The spread in precipitation seasonality (Figure 4a) is mainly driven by the spread in the precipitation during the monsoon season (Figure 4b). This is consistent with the fact that 71% of the precipitation falls during the monsoon season according to GPCP.

For the zonal wind seasonality, the SWING2 models show a strong spread over the TP and western China between 30°N and 45°N (Figure 4d). This corresponds to a region dominated by the westerlies in winter. Consistently, most of the spread in wind seasonality can be explained by the spread of winter winds (Figure 4f). This suggests

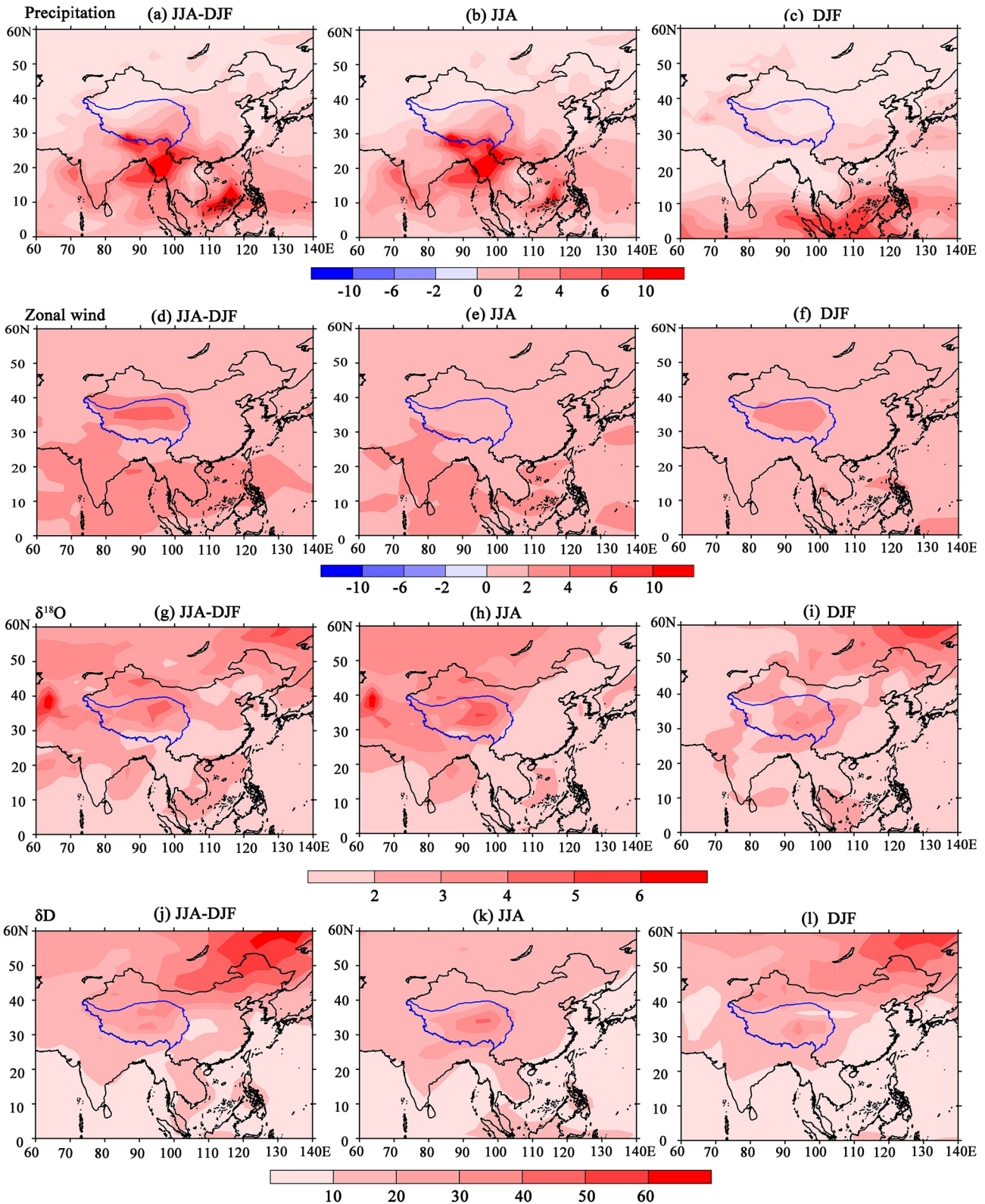


Figure 4. The inter-model standard deviation for the seasonality of precipitation rate (a), for summer precipitation rate (b in JJA), and for winter precipitation rate (c, in DJF). Same panels (a–c), but for zonal wind (d–f), precipitation $\delta^{18}\text{O}$ (g–i), and water vapor δD (j–l). The blue contour shows the boundary of the Tibetan Plateau (higher than 3,000 m).

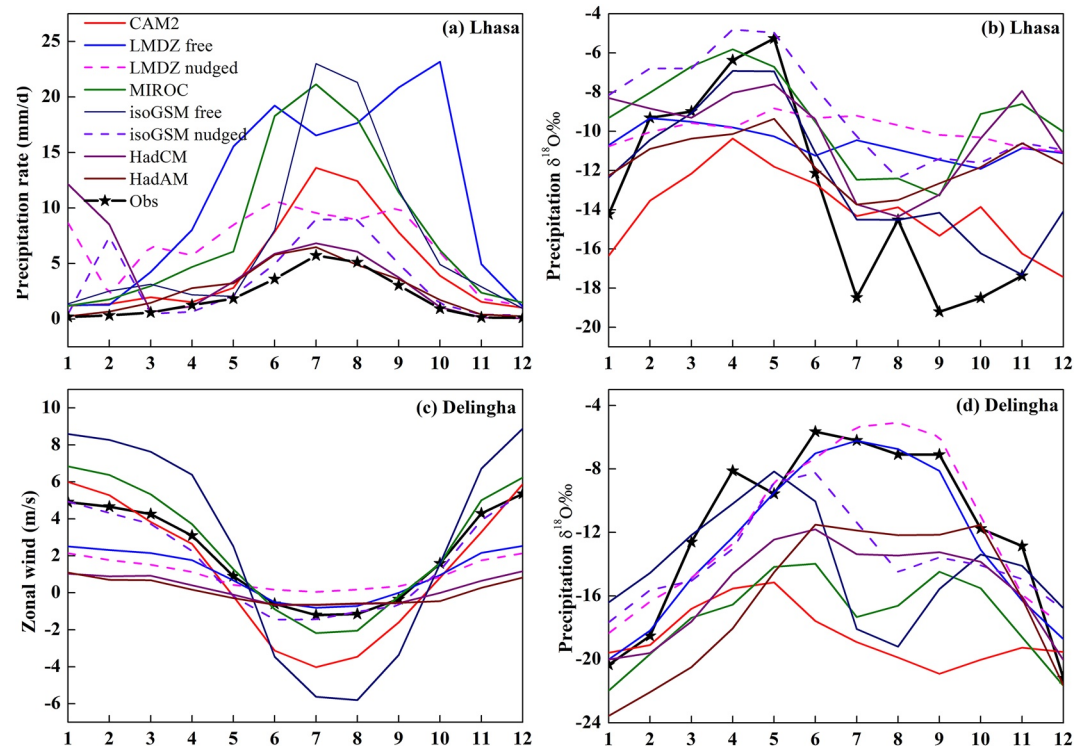


Figure 5. Seasonal cycle of multi-year-mean monthly-mean precipitation rate (mm/d) at Lhasa (a), weighted precipitation $\delta^{18}O$ (‰) at Lhasa (b), zonal wind (m/s) near the surface at Delingha (c), and weighted precipitation $\delta^{18}O$ (‰) at Delingha (d), for observations (black line with pentagram from different sources, see main text) and Stable Water Isotope Intercomparison Group 2 simulations. For a given color, solid and dashed lines represent free and nudged simulations, respectively.

that the model-data discrepancies in zonal winds are very diverse across the models. In addition, the zonal wind seasonality strongly varies with latitude in this region, with a maximum of around $35^{\circ}N$. The horizontally-striped pattern in Figure 4d suggests that models exhibit a spread at the latitudes where zonal wind seasonality is maximum (Figure 1f).

For the $\delta^{18}O_p$ seasonality, the models show a large spread over most of the southern TP, western TP, and northern India (Figure 4g). Since in summer air flows from the south as part of the monsoon flow (Figure 1a), the region with the maximum spread in $\delta^{18}O_p$ seasonality (Figure 4g) is located downstream of regions with the maximum spread in precipitation (Figure 4a). This suggests that the spread in precipitation seasonality in southern Asia contributes to the spread in $\delta^{18}O_p$ seasonality downstream. This would be consistent with previous studies indicating the role of rainfall over Southern Asia in the depletion of vapor and precipitation over the Tibetan Plateau (Gao et al., 2013; He et al., 2015). The spread in the north-western TP also coincides with the region of strong spread in zonal wind seasonality (Figure 4d). The spread in isotopic seasonality in the vapor (Figure 4j) shows results similar to those in the precipitation, but with the enhanced spread at higher latitudes. This strong spread is consistent with the strong spread already noticed across SWING2 models in Siberia (Gryazin et al., 2014).

In summary, the models can accurately capture the spatial patterns of meteorological variables and isotopic compositions in precipitation and vapor but underestimate its seasonality and show a significant spread around the multi-model mean. The sources of the inter-model spread will be analyzed in more detail in Section 4.

2.6. Seasonal Cycle at Representative Sites

Figure 5 depicts the multi-year-mean seasonal cycle of observed and simulated monthly-mean precipitation rates at Lhasa, zonal wind at Delingha and $\delta^{18}O_p$ at both sites. Simulated seasonal cycles at both sites are also evaluated with respect to observations using Taylor diagrams (Figures 6 and 7), a holistic evaluation for both the seasonal

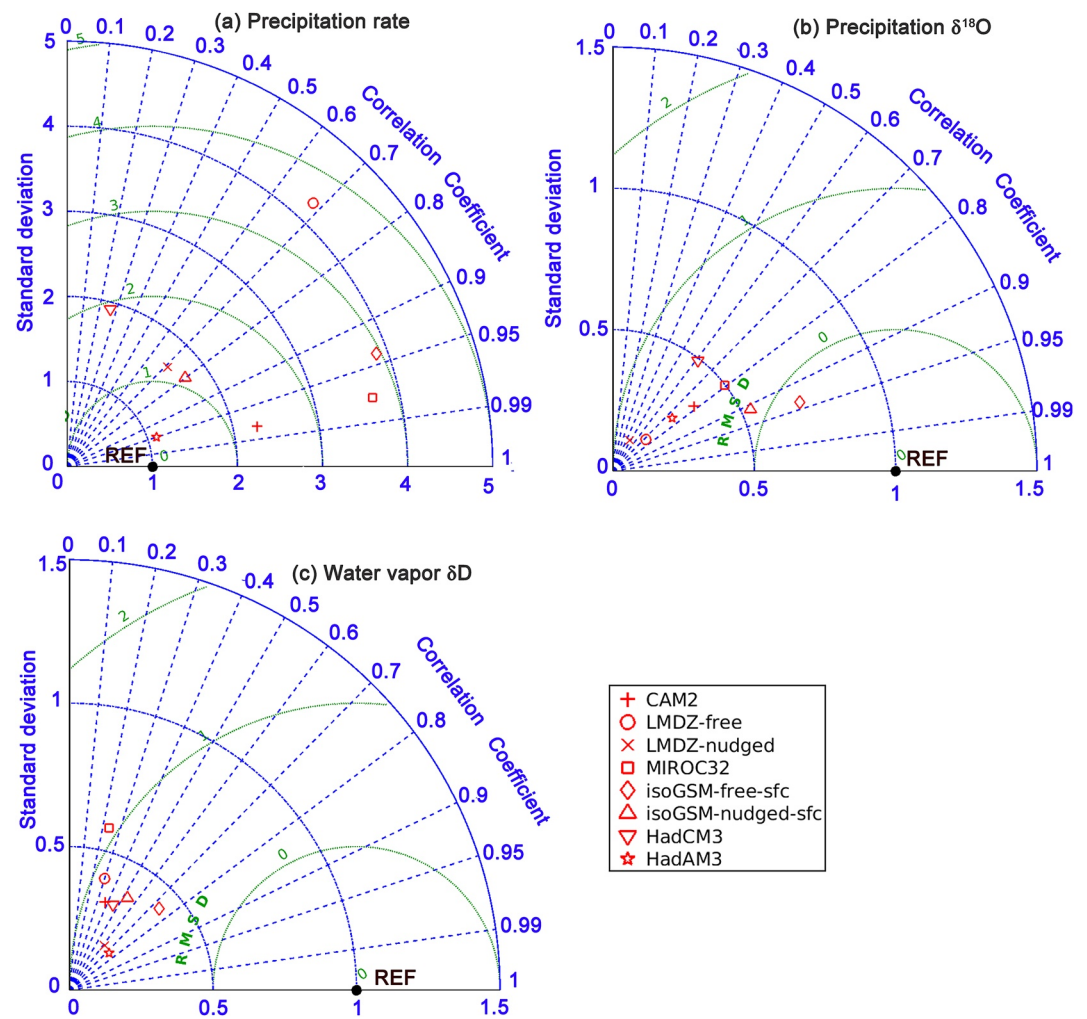


Figure 6. Taylor diagrams showing the performance of models in simulating the multi-year-mean monthly mean precipitation rate (mm/d) (a), weighted precipitation $\delta^{18}\text{O}$ (‰) (b), and water vapor δD (‰) (c) at Lhasa. The differently shaped boxes correspond to the different isotopic models. Correlations above 0.55 and 0.68 are statistically significant at $p < 0.05$ and $p < 0.01$.

amplitude and phase. Statistical indexes were calculated including the centered root-mean-square (RMS) error, standard deviation (SD), and correlation coefficient (r). A perfect match between estimated and simulated values would fall on the full-back dot in Figures 6 and 7. The precipitation $\delta^{18}\text{O}$ in GNIP, water vapor δD in TES, precipitation rate in GPCP, and zonal wind near the surface in NCEP-NCAR were used as reference data (black dot).

At Lhasa, observations show maximum precipitation in summer associated with the monsoon (Figure 5a). SWING2 models all simulate the maximum precipitation in summer except for the HadCM3, but occasionally with two peaks (e.g., LMDZ nudged) or with a delay (e.g., LMDZ free). Most models overestimate precipitation, with three models overpassing three for their normalized standard deviation (Figure 6a). The models without nudging are among those that overestimate precipitation the most (e.g., isoGSM free, MIROC32, LMDZ free).

Observed $\delta^{18}\text{O}_p$ at Lhasa strongly decreases by more than 10‰ from May to July, probably in response to the increased monsoonal precipitation along trajectories (Gao et al., 2013; He et al., 2015). $\delta^{18}\text{O}_p$ remains low until November (−17.38‰), and then progressively recovers until May (−5.26‰) (Figure 5b). Although the models simulate different $\delta^{18}\text{O}_p$ values in annual-mean, they all qualitatively capture the decrease of $\delta^{18}\text{O}$ during the monsoon season. However, all models underestimate the amplitude of the $\delta^{18}\text{O}_p$ seasonal cycle (Figure 6b). Five models exhibit a normalized standard deviation of smaller than 0.5 (Figure 6b). While nudged models show lower RMS for local precipitation, they do not necessarily show better skills for $\delta^{18}\text{O}_p$. For example, nudged

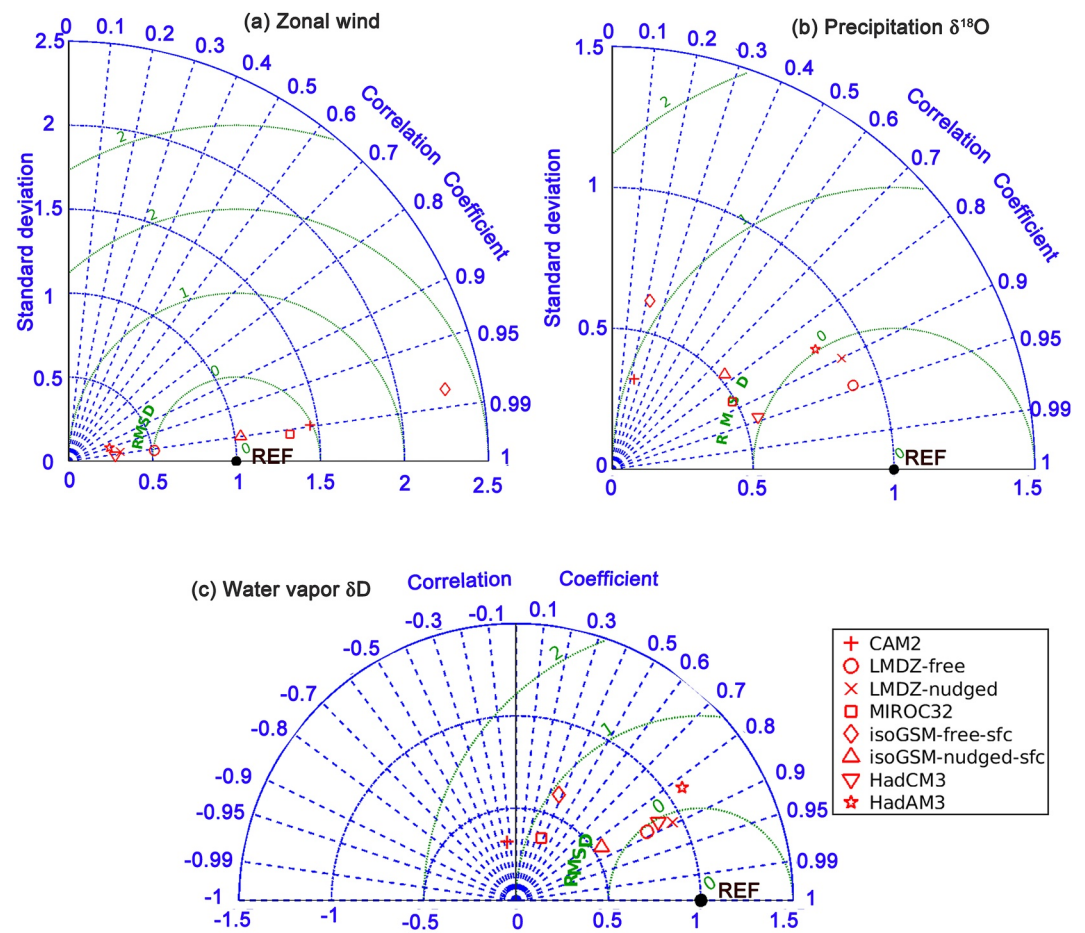


Figure 7. Same as Figure 6 but for Delingha, for zonal wind (m/s) near the surface (a), weighted precipitation $\delta^{18}\text{O}$ (‰) (b), water vapor δD (‰) (c).

LMDZ has the third lowest RMS for precipitation rate (Figure 6a, solid hexagon), but the highest RMS for $\delta^{18}\text{O}_p$ (Figure 6b). All models underestimate the δD_v compared to TES (Figure 6c). Yet, TES observations are expected to underestimate real seasonality, due to the limited sensitivity of TES retrievals (Section 2.2). This suggests that the reason why the SWING2 models underestimate the $\delta^{18}\text{O}$ seasonal variations of precipitation is that they underestimate the $\delta^{18}\text{O}_p$ seasonal variations of water vapor. Since the $\delta^{18}\text{O}$ of the vapor reflects the remote process, the models misrepresent remote processes affecting the vapor composition (e.g., large-scale circulation, convection along trajectories). In MA and JA, all models underestimate the $\delta^{18}\text{O}_p$ and δD_v (Figures S20b, S20c, S20e, S20f of Supporting Information S1), which is consistent with the underestimation of isotopic seasonal cycles (Figure 6). Moreover, the inter-annual variability is much smaller than the model-observation differences at Lhasa, especially for $\delta^{18}\text{O}_p$ and δD_v (Figure S20 of Supporting Information S1).

At Delingha, in the reanalysis, the wind blows from the West, as expected from its location in the westerly region, especially in winter (Figure 1b). The weakening of the summer winds shows some influence from the monsoon circulation. The models show a very large spread in the simulation of the atmospheric circulation, both in terms of annual-mean values, seasonal amplitudes, and shape of seasonal variations (Figure 5c and Figure 7a). The ratio of standard deviations ranges from about 0.3 to about 2.3 (Figure 7a). This is not surprising since horizontal winds are part of the large-scale circulation, which is strongly coupled to the distribution of precipitation (Yanai et al., 1973). It is thus expected that the spread in precipitation (Figure 4a) translates into a spread in horizontal winds (Figure 4b). We checked that the winter winds at Delingha significantly correlate with precipitation over the TP and India (Figure S24 of Supporting Information S1). In addition, over the TP, the large-scale circulation interacts with the topography (Yanai & Wu, 2006), whose representation strongly depends on the horizontal

resolution. Nudging the wind leads to a significant improvement in isoGSM, but not in LMDZ, maybe due to the coarse horizontal resolution.

Observed $\delta^{18}\text{O}_p$ at Delingha shows a maximum value in summer (Figure 5d). This is consistent with the temperature effect dominating $\delta^{18}\text{O}$ seasonal variations in the northern TP (Tian et al., 2007; Yao et al., 2013; Yu et al., 2006). Most models qualitatively capture the seasonal variations, but they all underestimate the seasonal amplitude (Figures 5d and Figure 7b). An underestimation of seasonal isotopic variability by SWING2 had already been noticed for mid-latitude sites compared to satellite observations (Risi et al., 2012b) and to precipitation observations in Siberia (Gryazin et al., 2014). Moreover, in JJA and DJF, we find that all models underestimate the isotopic variations of water vapor (Figures S21c, S21f of Supporting Information S1) while showing a large spread in simulating the precipitation $\delta^{18}\text{O}$ (Figures S21b, S21e of Supporting Information S1). Some models also show a hint of a summer depletion, as if the $\delta^{18}\text{O}_p$ responded to the monsoon precipitation as is the case in the southern TP. In particular, CAM2 shows a reversed seasonal cycle typical of the southern TP stations. The model skills to simulate the observed $\delta^{18}\text{O}_p$ are very similar to those for the simulated observed δD_v (Figure 7c). This supports our interpretation that in the northern TP, the reason why models underestimate the $\delta^{18}\text{O}$ seasonal variations is that they misrepresent remote processes.

We notice that at both Lhasa and Delingha and for the different variables, HadAM3 is more similar to HadCM3 than to any other simulations (Figure 5). This suggests that the physical representation of atmospheric processes is a larger source of a spread than boundary conditions.

In summary, most SWING2 models qualitatively capture the seasonal variations in $\delta^{18}\text{O}_p$ but underestimate their amplitude both in the southern and northern TP. In addition, they exhibit a very large spread in skills.

3. Interpreting Inter-Model Spread and Systematic Biases

The previous section has shown that there is a large spread in the simulation of the seasonal variation in $\delta^{18}\text{O}_p$ and that some models had significant biases compared to observations. In this section, we set two questions:

1. What drives this spread? Is the skill to simulate the isotopic composition driven by the skill to simulate the meteorological variables?
2. What are the causes of model biases?

3.1. Methodology

To address the question of the drivers of inter-model spread in isotopic composition, we look for “emergent constraints” for model skill at simulating isotopic seasonality. In the climate change community, “emergent constraints are physically explainable empirical relationships between characteristics of the current climate and long-term climate predictions that emerge in collections of climate model simulations (Klein & Hall, 2015). Emergent constraints allow to investigation of reasons for inter-model spread in climate models ensembles (e.g., Hall & Qu, 2006; Klein & Hall, 2015; Sherwood et al., 2014). Here we apply this concept of emergent constraints to investigate reasons for inter-model spread in the isotopic seasonality instead of long-term climate predictions. With this aim, we analyze correlations across models between the isotopic seasonality and metrics that reflect possible drivers (SI section1). In turn, understanding the drivers for inter-model spread can shed light on possible causes for model biases.

In Section 3.2, we found that two distinct regions show different isotopic seasonality. We will thus investigate them separately. We will focus here on understanding what controls the simulated seasonal variations in isotopic composition, rather than the simulated isotopic composition in the annual-mean, JJA or DJF. Indeed, the $\delta^{18}\text{O}_p$ in JJA significantly correlates with that in DJF in most regions (e.g., correlation of 0.7 in Lhasa, Figure S22 of Supporting Information S1). This means that the simulated seasonal-mean $\delta^{18}\text{O}_p$ is affected by annual-mean biases that are reflected in all seasons. In other words, each model has a basic state in annual-mean precipitation isotopic composition, and what controls this basic state is a different question that we consider beyond the scope of this paper. We define the seasonal variation of $\delta^{18}\text{O}_p$ as JA-MA in the southern TP and JJA-DJF in the northern TP, corresponding to extrema in $\delta^{18}\text{O}_p$ for these regions.

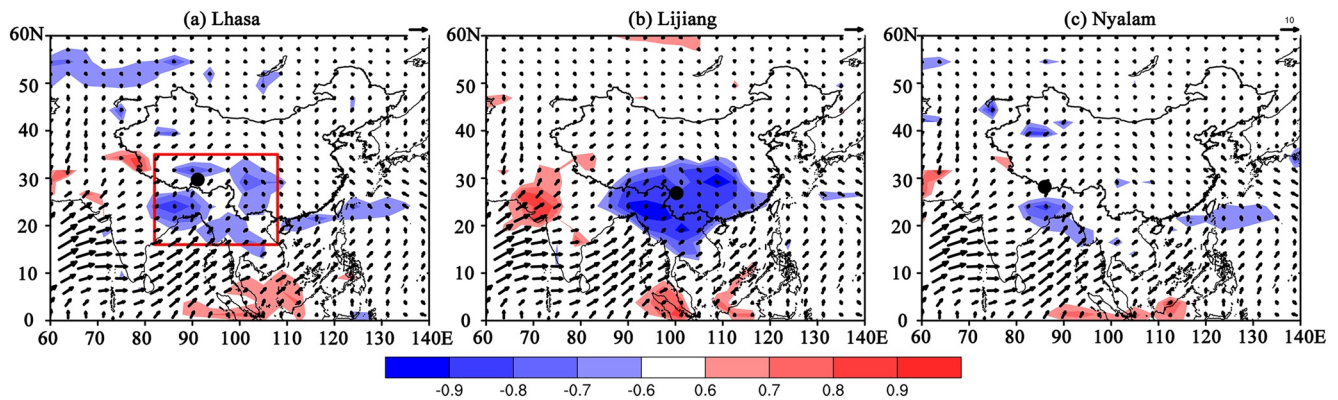


Figure 8. Correlation coefficients between precipitation $\delta^{18}\text{O}$ seasonality (‰) ($\Delta\delta^{18}\text{O}_p$, represented by JA-minus-MA difference) at a given site (a, Lhasa; b, Lijiang; c, Nyalam) and precipitation seasonality (ΔP_{ij}) (mm/d) at all grids (a)–(c). Only values that are significant at the two-tailed 95% confidence interval are plotted. The red rectangle for Lhasa is used to define the region in Figure 9. The JA winds as an overlay are shown (vector, m/s) near the surface. The correlation across models is calculated as follows, for example, for panel (a): let M be the number of simulations ($M = 8$). For each simulation m , with m from 1 to M , we calculate the $\delta^{18}\text{O}_p$ seasonality at Lhasa, $Y(m)$. Here by seasonality, we mean the multi-year mean of JA minus the multi-year mean of MA. Then for each model m , and for each grid box i, j , we calculate the precipitation seasonality, $X(m, (i), (j))$. Finally, for each grid box i, j , we calculate the correlation between $Y(m)$ and $X(m, (i), (j))$ across the M models, called $r(i), (j)$, and plot it as color shades.

3.2. The Southern Tibetan Plateau

Previous studies have highlighted the importance of upstream precipitation to control the isotope variations in the southern TP (Gao et al., 2013; He et al., 2015; Shi et al., 2020) at the seasonal and inter-annual time scales. One hypothesis is to explain the inter-model spread of isotopic seasonality in the southern TP is thus the spread in upstream precipitation.

If this hypothesis is valid, then we expect that models with the largest $\Delta\delta^{18}\text{O}_p$ at a given site of interest are those with the largest seasonality in upstream precipitation (ΔP). We thus expect a strong anti-correlation across models between $\Delta\delta^{18}\text{O}_p$ and ΔP_{ij} , where i, j are grid boxes that are located upstream of the site of interest.

Figure 8 shows the correlation maps between $\Delta\delta^{18}\text{O}_p$ at three representative stations (Lijiang, Nyalam, and Lhasa) and ΔP_{ij} (Figures 8a–8c). We find a patch of significantly negative correlation between $\Delta\delta^{18}\text{O}_p$ and ΔP_{ij} to the south of the stations (Figures 8a–8c), along air flows (Figures 1a and 1d), especially in Lijiang (Figure 8b). This supports our hypothesis that the spread in $\delta^{18}\text{O}_p$ seasonality is mainly driven by the spread in precipitation seasonality. This is consistent with the precipitation upstream trajectories controlling seasonal $\delta^{18}\text{O}_p$ variations in the southern TP (Gao et al., 2013; He et al., 2015; Midhun & Ramesh, 2016).

The results are similar for δD_v but with slightly lower correlations (not shown), probably due to the noisy aspect of the remote-sensing observations and the fact that they underestimate the δD_v seasonality.

To better visualize what controls the spread of $\delta^{18}\text{O}_p$ seasonality in the southern region, we show the $\delta^{18}\text{O}_p$ and δD_v seasonality as a function of mean precipitation seasonality in average over the region 16°N – 35°N , 82°E – 108°E . This region is defined according to the minimum negative correlation (red rectangle) in Figure 8. Horizontal averaging reduces the noise and thus increases the correlation. This is why the correlation in Figure 9 is much more negative compared to Figure 8. We find that models that have the largest $\delta^{18}\text{O}_p$ seasonality are those that have the largest precipitation seasonality in the upstream region (e.g., isoGSM free, MIROC32), with a negative correlation coefficient $r = -0.79$ ($p < 0.05$) (Figure 9a). Similarly, models that have the largest δD_v seasonality are those that have the largest precipitation seasonality in the upstream region, with a negative correlation coefficient $r = -0.43$ ($p > 0.05$) (Figure 9b). The lower correlation in water vapor could be explained by the contribution of post-condensational processes to strengthen the link between $\delta^{18}\text{O}_p$ and upstream precipitation across models, or by the noisier isotopic distribution observed by TES.

Figure 9a confirms that all models underestimate the seasonality of $\delta^{18}\text{O}_p$, in agreement with Figure 5b. However, not all models underestimate the seasonality of the precipitation rate: rather, three models overestimate it (Figure 9a). Even if a model had a perfect simulation of precipitation seasonality while lying on the regression line, it would still underestimate the $\delta^{18}\text{O}_p$ seasonality (i.e., CAM2). This suggests that the models

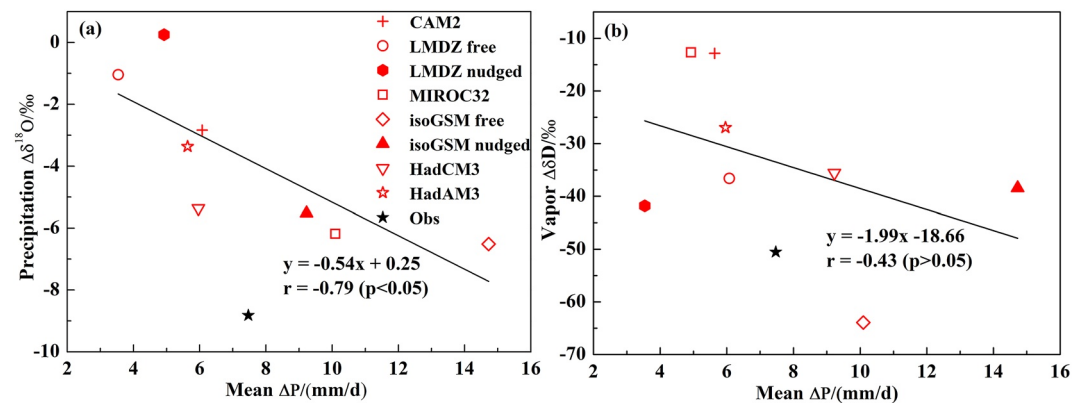


Figure 9. Relationship of precipitation $\delta^{18}\text{O}_p$ seasonality ($\Delta\delta^{18}\text{O}_p$) (‰) (a) and water vapor δD_v seasonality ($\Delta\delta\text{D}_v$) (‰) (b) at Lhasa as a function of mean upstream precipitation seasonality (ΔP) (16°N – 35°N , 82°E – 108°E , defined as the red rectangle in Figure 8a). The pentacle presents the observed value. The correlation coefficient varies from -0.73 to -0.87 between $\Delta\delta^{18}\text{O}_p$ and ΔP and from -0.34 to -0.59 between $\Delta\delta\text{D}_v$ and ΔP when we discard one of the 8 models each time.

are not sensitive enough to upstream precipitation. This is confirmed by the fact that the models underestimate the slope on average (Figure 9a). Several reasons may explain why models would underestimate the sensitivity of $\delta^{18}\text{O}_p$ to precipitation. It is $-0.5\text{‰}/\text{mm}\cdot\text{day}$ for observations (Figure 9a) and $-0.6 \pm 0.4\text{‰}/\text{mm}\cdot\text{day}$ for SWING2 models. For example, most models may underestimate the depleting effect of stratiform precipitation (Hu et al., 2018). Although the importance of stratiform portions of meso-scale convective systems for the latent heating profiles (Schumacher et al., 2004) and the isotopic composition (Aggarwal et al., 2016), they are not yet explicitly represented by GCMs (Rio et al., 2019). It is also possible that the model underestimates the depleting effect of convection because they do not explicitly organize mesoscale convective systems (Rio et al., 2019). It has been observed that convection depletes the water vapor more efficiently when it is organized into large and long-lived meso-scale convective systems (Lawrence et al., 2004; Maupin et al., 2021; Risi et al., 2008; Sengupta et al., 2020; Tremoy et al., 2014). Attempting to represent the convective organization in GCMs (Mapes & Neale, 2011) has not reached operationally-used GCMs. Alternatively, there could also be some local factors that lead the $\delta^{18}\text{O}_p$ seasonality to be more negative, and that requires a high spatial resolution to be captured (Shi et al., 2020).

In summary, the spread of upstream precipitation explains most of the spread of $\delta^{18}\text{O}_p$ seasonality, but there is still a systematic bias toward underestimated $\delta^{18}\text{O}_p$ seasonality. Therefore, some models can have a poor isotopic simulation even with a good precipitation simulation. Estimating in each model the fraction of the bias explained by the misrepresentation of the precipitation pattern would be very valuable from a model development perspective. Unfortunately, our framework cannot yield this estimate (SI Section 1 provides some mathematical background to justify this). However, some useful information could be obtained. For example, in the southern TP, we conclude that the models that underestimate the $\delta^{18}\text{O}_p$ seasonality the most are those that underestimate the precipitation rate seasonality the most. Thus, if a particular model underestimates the $\delta^{18}\text{O}_p$ seasonality, it is likely that it is due to its underestimation of the precipitation rate.

3.3. The Northern Tibetan Plateau

In Section 3.4, we have shown that in the northern TP, the observed $\delta^{18}\text{O}_p$ is higher in JJA than in DJF (about 13.7‰), that most models underestimate this amplitude, and that there is a significant spread in the simulated amplitude (Figures 6d and Figure 8). To better explore the mechanisms driving the simulated amplitude of the seasonal cycle of $\delta^{18}\text{O}_p$ and the spread across models, here we define the variation of JJA minus DJF as the seasonality in the northern region. To improve the knowledge of the models' capacity to capture isotopic seasonality, three typical stations, Hetian, Delingha, and Zhangye, are selected to assess the modeled results.

Various roles of climatic controls on precipitation isotopes such as the moisture sources (e.g., Kong et al., 2019; Tian et al., 2007, 2008; Yu et al., 2014), local temperature (Yu, Tian, et al., 2016) and convective activity (Guo et al., 2017) have been identified for the northern and northern-western TP. We thus calculated the correlations

Table 2
Statistical Correlations Between $\Delta\delta^{18}\text{O}_p$ at Delingha and the Seasonality in Temperature (ΔT), Specific Humidity (Δq), Water Vapor δD ($\Delta\delta D_v$) and Zonal Wind (ΔU) Averaged Over the Northern TP Region (32°N – 50°N , 75°E – 130°E)

	$\Delta\delta^{18}\text{O}_p$ versus ΔT	$\Delta\delta^{18}\text{O}_p$ versus Δq	$\Delta\delta^{18}\text{O}_p$ versus $\Delta\delta D_v$	$\Delta\delta^{18}\text{O}_p$ versus ΔU
Slope	−0.21	−0.07	3.25	0.27
Correlation coefficient (r)	−0.41	−0.26	0.59	0.92**

Note. The correlation coefficient (r) varies from −0.22 to −0.37 between $\Delta\delta^{18}\text{O}_p$ and Δq , from 0.41 to 0.66 between $\Delta\delta^{18}\text{O}_p$ and $\Delta\delta D_v$ and from 0.89 to 0.95 between $\Delta\delta^{18}\text{O}_p$ and ΔU when we discard one of the 8 models each time. The r varies from −0.04 to −0.45 between $\Delta\delta^{18}\text{O}_p$ and ΔT , only when the CAM2 is removed, the r is −0.82.

** Correction is significant at the 0.01 confidence limit.

between $\Delta\delta^{18}\text{O}_p$ and meteorological factors. In Table 2, we take Delingha as an example. We average the meteorological variables over the surrounding region that maximize the correlations with at least one meteorological variable. This region was found to be 32°N – 50°N , 75°E – 130°E). The positive correlation between $\Delta\delta^{18}\text{O}_p$ and $\Delta\delta D_v$, with an r value of 0.59 (Table 2) indicates that the variability of $\delta^{18}\text{O}_p$ is not related to the local post-condensation process, but rather to remote processes. We find that $\Delta\delta^{18}\text{O}_p$ is not significantly related to the simulated seasonality of temperature (ΔT). In the absence of rain evaporation and for a given moisture source, the isotopic ratios of water vapor and subsequent precipitation are expected to decrease as specific humidity q decreases, either following Rayleigh distillation, or following mixing lines that connect different points along the Rayleigh distillation line (Galewsky & Hurley, 2010; Noone, 2012; Worden et al., 2007). If Rayleigh distillation or mixing lines were controlling the simulated $\Delta\delta^{18}\text{O}_p$, then we would expect a high correlation between simulated $\Delta\delta^{18}\text{O}_p$ and Δq ; models that overestimate Δq the most would also overestimate $\Delta\delta^{18}\text{O}_p$ the most. However, this is not the case (Table 2). This shows that rain evaporation, or different air mass origins or moisture sources, drives the inter-model spread in simulated $\Delta\delta^{18}\text{O}_p$. We find a significant relationship with the zonal wind (ΔU) ($r = 0.92$, $p < 0.01$). This suggests that the spread of isotope seasonality in the northern TP region is likely due to the spread of the simulated large-scale circulation, and thus to the spread of air mass origins.

To investigate the effect of large-scale circulation in more detail, in Figure 10 we plot the inter-model correlations between $\Delta\delta^{18}\text{O}_p$ and $\Delta\delta D_v$ at a given site and the regional zonal wind seasonality. At Delingha and Zhangye, $\delta^{18}\text{O}_p$ seasonality positively correlates with zonal wind seasonality to the west of the sites, along trajectories from

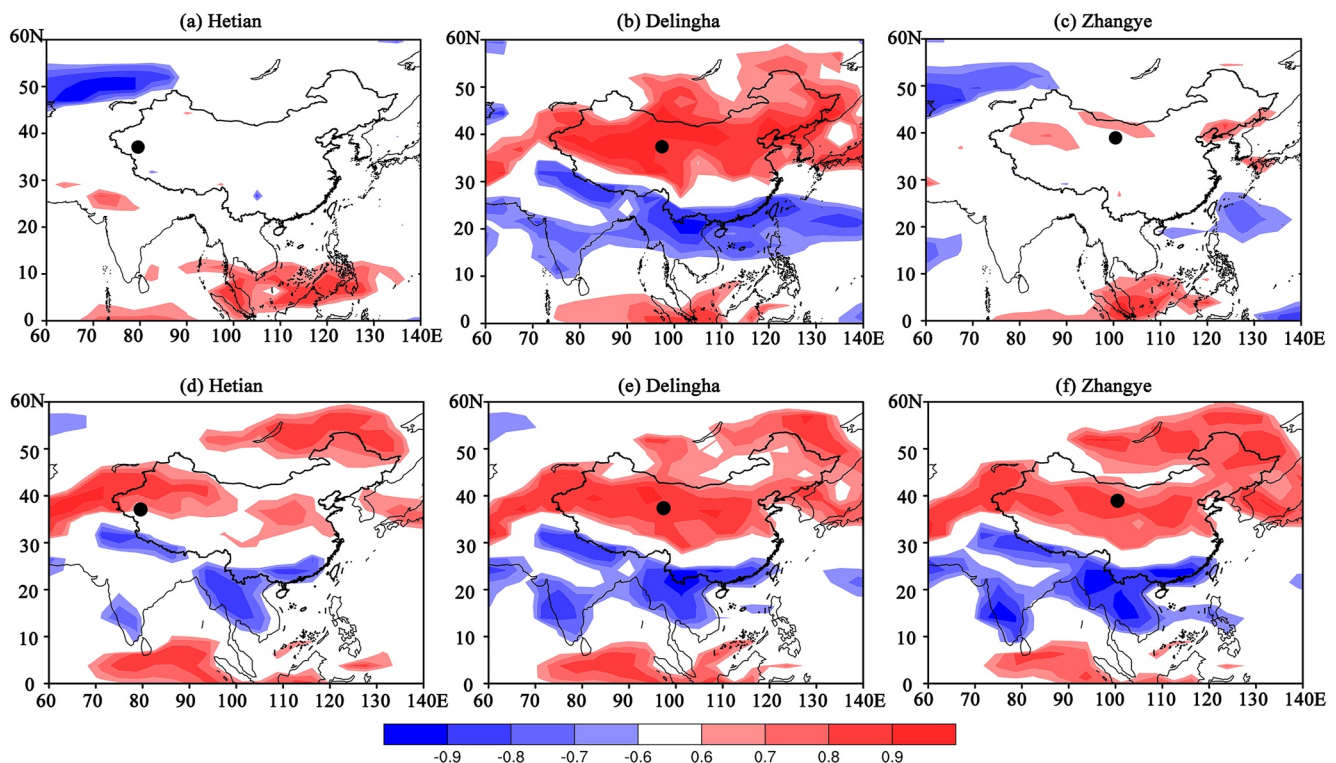


Figure 10. Correlation coefficients between precipitation $\delta^{18}\text{O}$ seasonality ($\Delta\delta^{18}\text{O}_p$, represented by the JJA-minus-DJF difference) and water vapor $\Delta\delta D$ seasonality ($\Delta\delta D_v$) at a given site (a), (d) Hetian, (b), (e) Delingha, (c), (f) Zhangye and zonal wind seasonality (ΔU) near the surface at all grids. Only values that are significant at the two-tailed 95% confidence interval are plotted. The blue rectangle for Delingha is used to define the region in Figure 11 and Table 2.

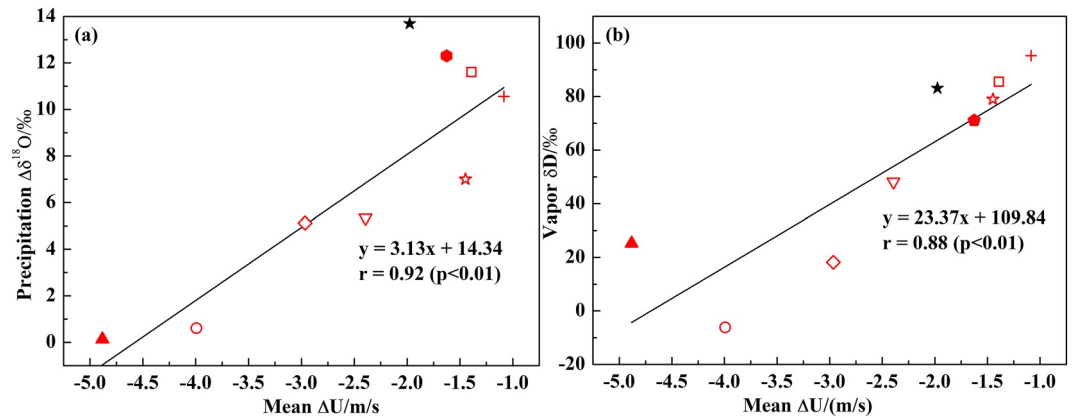


Figure 11. Relationship of precipitation $\delta^{18}\text{O}_p$ (a) and water vapor δD (b) at Delingha as a function of mean zonal wind seasonality (ΔU) (32°N – 50°N – 75°E – 130°E , defined as the blue rectangle in Figure 10b). The black star presents the observed value from NCEP–NCAR reanalysis. The correlation coefficient varies from 0.89 to 0.95 between $\Delta\delta^{18}\text{O}_p$ and ΔU and from 0.85 to 0.99 between $\Delta\delta\text{D}_v$ and ΔU when we discard one of the eight models each time. The observed zonal winds from ERA5 are almost the same (Figure S16).

the upstream regions, especially at Delingha. This shows that the models that have the largest $\Delta\delta^{18}\text{O}_p$ are those that have the smallest zonal wind seasonality in the upstream regions.

To better visualize what controls the spread of precipitation $\delta^{18}\text{O}$ seasonality in the northern region, we again take Delingha as an example. In Figure 11, we plot $\Delta\delta^{18}\text{O}_p$ as a function of the zonal wind seasonality on average over 32°N – 50°N – 75°E – 130°E . This region corresponds to the maximum correlation in Figure 10. Our analysis shows that $\Delta\delta^{18}\text{O}_p$ at Delingha is positively correlated with the zonal wind ($r = 0.92$, Figure 11a). We also observe a similar correlation with $\Delta\delta\text{D}_v$ (Figure 11b).

What mechanism links the zonal wind seasonality to the $\delta^{18}\text{O}_p$ seasonality? In JJA, the air slightly flows from east to west as the monsoon flow is deflected by the topography (Figure 1a). In DJF, air flows from the west, as part of the westerlies (Figure 1b). Therefore, the JJA–minus–DJF difference of the zonal wind is generally negative in the northern region (Figure 1c). If in a given model, the monsoon circulation extends further north (orange on Figure 12b), then the westerly airflow is weaker than normal in JJA (cyan in Figure 12), which leads to more negative zonal wind seasonality. At the same time, the vapor isotope in JJA is more depleted (purple in Figure 12) because more vapor comes from the monsoon convective region, leading to weaker $\delta^{18}\text{O}_p$ seasonality. This is what we see for example, in CAM2 (Figure S18a of Supporting Information S1). In contrast, if in a given model the monsoon circulation extends to fewer northerly latitudes, then the westerly flow is less reduced compared to DJF, and the wind seasonality is thus less negative (Figure 12c). At the same time, less vapor comes from the monsoon flow, leading to a stronger $\delta^{18}\text{O}_p$ seasonality. This is what we see for example, in isoGSM (Figure S18b of Supporting Information S1). The influence of the depletion by convection along the monsoon flow is probably what explains the absence of correlation between $\Delta\delta^{18}\text{O}_p$ and Δq . The importance of the relative contribution of different air mass origins is consistent with previous studies (Tian et al., 2001).

Due to the coarse resolution of SWING2 models and the strong altitude effect in mountain regions, we expected that some of the biases in simulated $\delta^{18}\text{O}_p$ could be due to the bias in topography. We checked however that there was no correlation between the bias in $\delta^{18}\text{O}_p$ and the bias in topography, neither at Lhasa nor at Delingha (Figure S26 of Supporting Information S1), neither in summer nor in winter. Therefore, the biases in topography do not contribute to the biases in $\delta^{18}\text{O}_p$.

To summarize, the spread of $\Delta\delta^{18}\text{O}_p$ is mostly controlled by the spread of zonal wind, reflecting the seasonal contrast in moisture sources (Figure 12). However, compared to observations, all models underestimate the seasonality of $\delta^{18}\text{O}_p$, but not all underestimate the seasonality of zonal wind, so there is also a systematic bias that is unrelated to the simulation of wind.

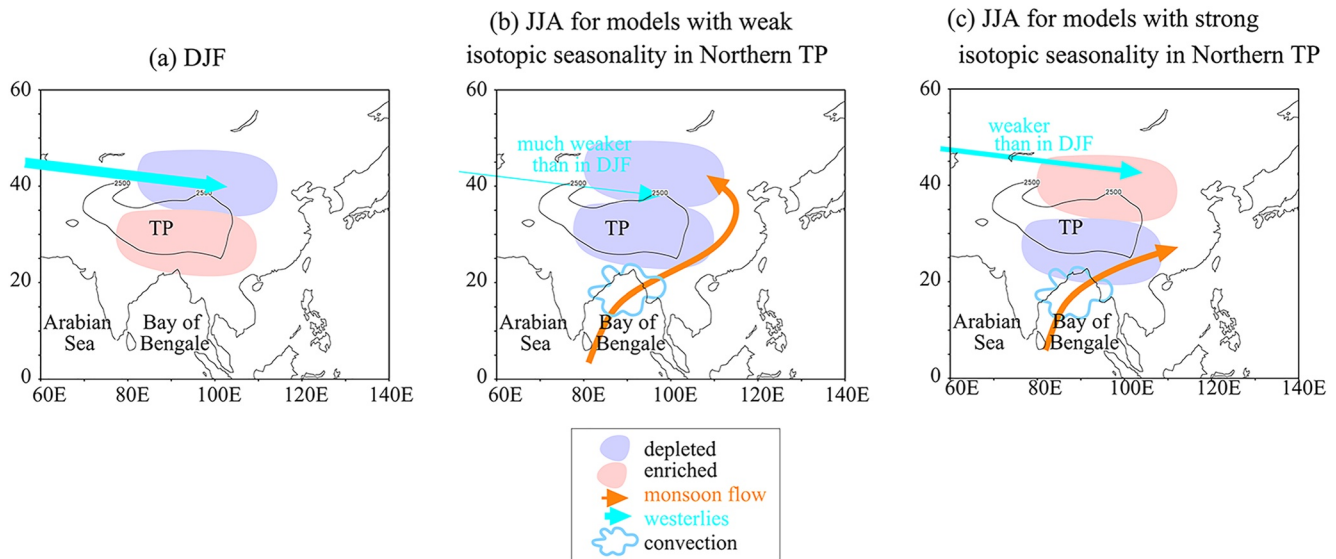


Figure 12. Schematic illustrating how the zonal wind seasonality affects the precipitation $\delta^{18}\text{O}$ seasonality in the Northern Tibetan Plateau (TP). (a) In DJF, the westerlies are the major wind flow. The precipitation is depleted in northern TP and enriched in southern TP. (b) In JJA, for models with a weak seasonality in the northern TP, the monsoon flow brings water vapor depleted by convection and the westerlies are much weaker than in DJF. (c) In JJA, for models with a weak seasonality in the northern TP, the monsoon flow brings water vapor depleted by convection to fewer northerly altitudes, and the westerlies are just slightly weaker than in DJF.

4. Paleoclimate Implications

We have shown that the SWING2 models reproduce well the present-day seasonality of $\delta^{18}\text{O}_p$ (JJA-minus-DJF), but they underestimate it to various extents in both the southern and northern TP. What are the expected consequences of the model biases that we have identified on the skill of models to capture past $\delta^{18}\text{O}_p$ changes?

In southern TP and south-western China, glaciers and speleothems show more depleted multi-annual-mean precipitation during the mid-Holocene (MH), 6 000 years ago, than at present (Cai et al., 2012; Cheng et al., 2006; Thompson et al., 1997; Y.J. Wang et al., 2001). This observed signal is very spatially coherent across the southern pan-Asia region (Hu et al., 2019). The most common interpretation for this depletion is that during MH, the summer insolation in the Northern Hemisphere was stronger, leading to more active Asian monsoons associated with more precipitation upstream air mass trajectories (Y.J. Wang et al., 2001). As such, there are similarities between the mechanisms for MH-minus-present $\delta^{18}\text{O}_p$ changes and JJA-minus-DJF $\delta^{18}\text{O}_p$ changes. General circulation models often underestimate the $\delta^{18}\text{O}_p$ changes from present-day to MH in the southern part of the TP (Comas-Bru et al., 2019; Risi et al., 2010). For example, the $\delta^{18}\text{O}_p$ decreases by about 2.5‰ in the Guliya ice core from PI to MH (Thompson et al., 2000) and by about two‰ in Chinese speleothems (Y. Wang et al., 2008). By comparison, the $\delta^{18}\text{O}_p$ changes simulated by GCMs range from a 1‰ or 2‰ decrease (LeGrande & Schmidt, 2009; Risi et al., 2010; Schmidt et al., 2007) to a 2‰ increase (Comas-Bru et al., 2019). This large spread and the tendency for underestimating the $\delta^{18}\text{O}_p$ decrease from PI to MH is reminiscent of the large spread and tendency for underestimating the $\delta^{18}\text{O}_p$ decrease for the present from DJF to JJA.

It has been shown that even models that correctly simulate the precipitation seasonality underestimate the $\delta^{18}\text{O}_p$ seasonality (Figure 10a). One possible reason for this is that models systematically underestimate the isotopic response to upstream precipitation. If this also holds true for MH as well, then even models that correctly simulate the precipitation increase from PI to MH would still underestimate the $\delta^{18}\text{O}_p$ decrease from PI to MH. We quantify that this could contribute to the underestimation of the simulated $\delta^{18}\text{O}_p$ decrease from PI to MH of more than 1‰ (SI Section 2). This is of the same order of magnitude as the underestimate in most GCMs. In addition, the large inter-model spread in the precipitation- $\delta^{18}\text{O}_p$ slope (Figure 9a) could be responsible for the large inter-model spread in the simulated MH-PI $\delta^{18}\text{O}_p$ difference.

We also explored several other hypotheses that may connect model-data discrepancies at orbital and seasonal time scales, including the underestimated precipitation change from MH to PI and the underestimated seasonality

effect, but these mechanisms have a marginal impact (SI Section 2). Note that here we simply made simple back-of-the-envelope calculations. To further test and quantify these hypotheses, extending SWING2 to include paleoclimate simulations would be useful to investigate the link between orbital and seasonal variations across different models.

To conclude, a recommendation of this study is to evaluate the simulated precipitation- $\delta^{18}\text{O}_p$ slope at the seasonal scale before applying a GCM at the orbital time scale, to be aware of the possible impact on the simulated orbital changes of $\delta^{18}\text{O}_p$.

5. Conclusions

In this study, we use eight simulations from SWING2 models to explore what controls the skill of general circulation models to simulate the seasonal cycle of water isotopic composition over the TP region.

The comparison between observations and models indicates that the SWING2 models perform well with regards to the spatial pattern of the water stable isotope of the precipitation and vapor over the TP region, but there exists significant inter-model spread and systematic biases, with notably an underestimated seasonality. Our results emphasize that the inter-model spread of isotopes is largely related to inter-model spread of the physical aspects of the climate. Inter-model spread of isotopic seasonality is primarily driven by the spread of upstream precipitation in the southern TP region, whereas the westerlies dominate the inter-spread of the isotope in the northern TP region.

Therefore, we conclude that for a GCM to simulate isotopes well, it needs to simulate the climate well. However, even a model with a perfect climate would not necessarily have a perfect isotopic simulation.

What are the consequences of model biases on the simulation of isotopic composition for past climates? Does it affect our interpretation of $\delta^{18}\text{O}$ in glaciers or speleothems based on GCM simulations? We suggest that if GCMs underestimate the isotopic response to precipitation changes at the seasonal scale for the present and if this discrepancy holds at orbital time scales, then this would contribute to the underestimated $\delta^{18}\text{O}$ decrease from the present to mid-Holocene. Extending SWING2 to include paleoclimate simulations would be useful to check this hypothesis.

Data Availability Statement

These datasets were used in this study: the SWING2 simulations outputs (Risi et al., 2012a, available at <https://data.giss.nasa.gov/swing2/>), the GNIP dataset (IAEA/WMO, 2006, available at <https://www.iaea.org/services/networks/gnip>), TES retrievals (Worden et al., 2006, 2007, available at <https://cmr.earthdata.nasa.gov/search%20concepts/C1000000361-LARC.html>), the GPCP and TRMM precipitation datasets (Adler et al., 2018, available at <http://gpcp.umd.edu/> and Huffman et al., 2010, https://disc.gsfc.nasa.gov/datasets/TRMM_3B42RT_Daily_7/summary, respectively), the NCEP-NCAR and ERA5 reanalysis datasets (Kalnay et al., 1996, available at <https://psl.noaa.gov/data/gridded/data.ncep.reanalysis.html> and Copernicus Climate Change Service (C3S), 2017, <https://cds.climate.copernicus.eu/cdsapp%23%21/dataset/reanalysis%2Dera5%2Dland%2Dmonthly%2Dmeans%3Ftab%3Doverview>, respectively), the IMD dataset (Pai et al., 2015, available at <https://iridl.ideo.columbia.edu/SOURCES/IMD/RF0p25/>) and GOTOP020 dataset (U.S. Geological Survey, available at <https://www.usgs.gov/centers/eros>).

References

- Adler, R. F., Sapiano, M. R., Huffman, G. J., Wang, J. J., Gu, G., Bolvin, D., et al. (2018). The Global Precipitation Climatology Project (GPCP) monthly analysis (new version 2.3) and a review of 2017 global precipitation. *Atmosphere*, 9(4), 138. <https://doi.org/10.3390/atmos9040138>
- Aggarwal, P. K., Romatschke, U., Araguas-Araguas, L., Belachew, D., Longstaffe, F. J., Berg, P., et al. (2016). Proportions of convective and stratiform precipitation revealed in water isotope ratios. *Nature Geoscience*, 9(8), 624–629. <https://doi.org/10.1038/ngeo2739>
- An, W., Hou, S., Zhang, Q., Zhang, W., Wu, S., Xu, H., et al. (2017). Enhanced recent local moisture recycling on the northwestern Tibetan Plateau deduced from ice core deuterium excess records. *Journal of Geophysical Research: Atmospheres*, 122(23), 12–541. <https://doi.org/10.1002/2017jd027235>
- An, W., Hou, S., Zhang, W., Wu, S., Xu, H., Pang, H., et al. (2016). Possible recent warming hiatus on the northwestern Tibetan Plateau derived from ice core records. *Scientific Reports*, 6(1), 1–8. <https://doi.org/10.1038/srep32813>
- Araguás-Araguás, L., Froehlich, K., & Rozanski, K. (1998). Stable isotope composition of precipitation over southeast Asia. *Journal of Geophysical Research*, 103(D22), 28721–28742. <https://doi.org/10.1029/98jd02582>

Acknowledgments

This research was supported by the National Natural Science Foundation of China (42101044, 42077188, 52109007, and 41901095) and the Youth Innovation Promotion Association of CAS (2020067). We thank all SWING2 members for producing and making available their model outputs. SWING2 was supported by the Isotopic Hydrology Program at the International Atomic Energy Agency.

- Bershaw, J., Penny, S. M., & Garzione, C. N. (2012). Stable isotopes of modern water across the Himalaya and eastern Tibetan Plateau: Implications for estimates of paleoelevation and paleoclimate. *Journal of Geophysical Research*, *117*(D2), 1–18. <https://doi.org/10.1029/2011jd016132>
- Bony, S., Risi, C., & Vimeux, F. (2008). Influence of convective processes on the isotopic composition ($\delta^{18}\text{O}$ and δD) of precipitation and water vapor in the tropics: 1. Radiative-convective equilibrium and tropical ocean–global atmosphere–coupled ocean–atmosphere response experiment (TOGA-COARE) simulations. *Journal of Geophysical Research*, *113*(D19), D19305. <https://doi.org/10.1029/2008jd009942>
- Botsyun, S., Sepulchre, P., Donnadieu, Y., Risi, C., Licht, A., & Rugenstein, J. K. C. (2019). Revised paleoaltimetry data show low Tibetan Plateau elevation during the Eocene. *Science*, *363*(6430), 1436. <https://doi.org/10.1126/science.aag1436>
- Breitenbach, S. F., Adkins, J. F., Meyer, H., Marwan, N., Kumar, K. K., & Haug, G. H. (2010). Strong influence of water vapor source dynamics on stable isotopes in precipitation observed in Southern Meghalaya, NE India. *Earth and Planetary Science Letters*, *292*(1–2), 212–220. <https://doi.org/10.1016/j.epsl.2010.01.038>
- Bühler, J. C., Roesch, C., Kirschner, M., Sime, L., Holloway, M. D., & Rehfeld, K. (2020). Comparison of the oxygen isotope signatures in speleothem records and HadCM3 model simulations for the last millennium. *Climate of the Past Discussions*, 1–30.
- Cai, Y., Zhang, H., Cheng, H., An, Z., Edwards, R. L., Wang, X., et al. (2012). The Holocene Indian monsoon variability over the southern Tibetan Plateau and its teleconnections. *Earth and Planetary Science Letters*, *335*, 135–144. <https://doi.org/10.1016/j.epsl.2012.04.035>
- Cai, Z., & Tian, L. (2020). What causes the postmonsoon O-18 depletion over bay of bengal head and beyond? *Geophysical Research Letters*, *47*(4), e2020GL086985. <https://doi.org/10.1029/2020gl086985>
- Che, Y., Zhang, M., Wang, S., Wang, J., Liu, Y., & Zhang, F. (2016). Stable water isotopes of precipitation in China simulated by SWING2 models. *Arabian Journal of Geosciences*, *9*(19), 1–12. <https://doi.org/10.1007/s12517-016-2755-5>
- Chen, B., Xu, X. D., Yang, S., & Zhang, W. (2012). On the origin and destination of atmospheric moisture and air mass over the Tibetan Plateau. *Theoretical and Applied Climatology*, *110*(3), 423–435. <https://doi.org/10.1007/s00704-012-0641-y>
- Cheng, H., Edwards, R. L., Wang, Y., Kong, X., Ming, Y., Kelly, M. J., et al. (2006). A penultimate glacial monsoon record from Hulu Cave and two-phase glacial terminations. *Geology*, *34*(3), 217–220. <https://doi.org/10.1130/g22289.1>
- Codron, F., & Sadourny, R. (2002). Saturation limiters for water vapour advection schemes: Impact on orographic precipitation. *Tellus A*, *54*(4), 338–349.
- Comas-Bru, L., Harrison, S. P., Werner, M., Rehfeld, K., Mahjoor, L. A., & Veiga-Pires, C. (2019). Evaluating model outputs using integrated global speleothem records of climate change since the last glacial. *Climate of the Past*, *15*(4), 1557–1579. <https://doi.org/10.5194/cp-15-1557-2019>
- Copernicus climate change Service (C3S). (2017). ERA5: Fifth generation of ECMWF atmospheric reanalyses of the global climate [Dataset]. Copernicus Climate Change Service Climate Data Store (CDS). Retrieved from <https://cds.climate.copernicus.eu/cdsapp#!/home>
- Dansgaard, W. (1964). Stable isotopes in precipitation. *Tellus*, *16*(4), 436–468. <https://doi.org/10.1111/j.2153-3490.1964.tb00181.x>
- Dee, S. G., Nusbaumer, J., Bailey, A., Russell, J. M., Lee, J. E., Konecky, B., et al. (2018). Tracking the strength of the Walker Circulation with stable isotopes in water vapor. *Journal of Geophysical Research: Atmospheres*, *123*(14), 7254–7270. <https://doi.org/10.1029/2017jd027915>
- Del Genio, A. D. (2012). Representing the sensitivity of convective cloud systems to tropospheric humidity in general circulation models. *Surveys in Geophysics*, *33*(3–4), 637–656. <https://doi.org/10.1007/s10712-011-9148-9>
- Feng, R., Poulsen, C. J., Werner, M., Chamberlain, C. P., Mix, H. T., & Mulch, A. (2013). Early Cenozoic evolution of topography, climate, and stable isotopes in precipitation in the North American Cordillera. *American Journal of Science*, *313*(7), 613–648. <https://doi.org/10.2475/07.2013.01>
- Field, R. D., Kim, D., LeGrande, A. N., Worden, J., Kelley, M., & Schmidt, G. A. (2014). Evaluating climate model performance in the tropics with retrievals of water isotopic composition from Aura TES. *Geophysical Research Letters*, *41*(16), 6030–6036. <https://doi.org/10.1002/2014gl060572>
- Galewsky, J., & Hurley, J. V. (2010). An advection-condensation model for subtropical water vapor isotopic ratios. *Journal of Geophysical Research*, *115*(D16), D16116. <https://doi.org/10.1029/2009jd013651>
- Gao, J., Masson-Delmotte, V., Risi, C., He, Y., & Yao, T. (2013). What controls precipitation $\delta^{18}\text{O}$ in the southern Tibetan plateau at seasonal and intra-seasonal scales? A case study at Lhasa and Nyalam. *Tellus B: Chemical and Physical Meteorology*, *65*(1), 21043. <https://doi.org/10.3402/tellusb.v65i0.21043>
- Gao, J., Risi, C., Masson-Delmotte, V., He, Y., & Xu, B. (2016). Southern Tibetan Plateau ice core $\delta^{18}\text{O}$ reflects abrupt shifts in atmospheric circulation in the late 1970s. *Climate Dynamics*, *46*(1–2), 291–302. <https://doi.org/10.1007/s00382-015-2584-3>
- Gates, W. L. (1992). Amip: The atmospheric model intercomparison project. *Bulletin of the American Meteorological Society*, *73*(12), 1962–1970. [https://doi.org/10.1175/1520-0477\(1992\)073<1962:atamip>2.0.co;2](https://doi.org/10.1175/1520-0477(1992)073<1962:atamip>2.0.co;2)
- Gryazin, V., Risi, C., Jouzel, J., Kurita, N., Worden, J., Frankenberg, C., et al. (2014). The added value of water isotopic measurements for understanding model biases in simulating the water cycle over Western Siberia. *Atmospheric Chemistry and Physics Discussion*, *14*, 4457–4503. <https://doi.org/10.5194/acp-14-9807-2014>
- Guo, X., Tian, L., Wen, R., Yu, W., & Qu, D. (2017). Controls of precipitation $\delta^{18}\text{O}$ on the northwestern Tibetan plateau: A case study at Ngari station. *Atmospheric Research*, *189*, 141–151. <https://doi.org/10.1016/j.atmosres.2017.02.004>
- Gusain, A., Ghosh, S., & Karmakar, S. (2020). Added value of CMIP6 over CMIP5 models in simulating Indian summer monsoon rainfall. *Atmospheric Research*, *232*, 104680. <https://doi.org/10.1016/j.atmosres.2019.104680>
- Hall, A., & Qu, X. (2006). Using the current seasonal cycle to constrain snow albedo feedback in future climate change. *Geophysical Research Letters*, *33*(3), L03502. <https://doi.org/10.1029/2005GL025127>
- He, Y., Risi, C., Gao, J., Masson-Delmotte, V., Yao, T., Lai, C. T., et al. (2015). Impact of atmospheric convection on south Tibet summer precipitation isotopologue composition using a combination of in situ measurements, satellite data, and atmospheric general circulation modeling. *Journal of Geophysical Research: Atmospheres*, *120*(9), 3852–3871. <https://doi.org/10.1002/2014jd022180>
- Hren, M. T., Bookhagen, B., Blisniuk, P. M., Booth, A. L., & Chamberlain, C. P. (2009). $\delta^{18}\text{O}$ and δD of streamwaters across the Himalaya and Tibetan Plateau: Implications for moisture sources and paleoelevation reconstructions. *Earth and Planetary Science Letters*, *288*(1–2), 20–32. <https://doi.org/10.1016/j.epsl.2009.08.041>
- Hu, J., Emile-Geay, J., Nusbaumer, J., & Noone, D. (2018). Impact of convective activity on precipitation $\delta^{18}\text{O}$ in isotope-enabled general circulation models. *Journal of Geophysical Research: Atmospheres*, *123*(23), 13–595. <https://doi.org/10.1029/2018jd029187>
- Hu, J., Emile-Geay, J., Tabor, C., Nusbaumer, J., & Partin, J. (2019). Deciphering oxygen isotope records from Chinese speleothems with an isotope-enabled climate model. *Paleoceanography and Paleoclimatology*, *34*(12), 2098–2112. <https://doi.org/10.1029/2019PA003741>
- Huffman, G. J., Adler, R. F., Bolvin, D. T., & Nelkin, E. J. (2010). The TRMM multi-satellite precipitation analysis (TMPA). In M. Gebremichael, & F. Hossain (Eds.), *Satellite rainfall Applications for surface Hydrology*. Springer. https://doi.org/10.1007/978-90-481-2915-7_1
- IAEA/WMO. (2006). Isotope Hydrology Information System, The ISOHIS Database [Dataset]. IAEA/WMO. Retrieved from <http://www.iaea.org/water>

- Ishizaki, Y., Yoshimura, K., Kanae, S., Kimoto, M., Kurita, N., & Oki, T. (2012). Interannual variability of H₂¹⁸O in precipitation over the Asian monsoon region. *Journal of Geophysical Research*, 117(D16). <https://doi.org/10.1029/2011jd015890>
- Jia, K., Ruan, Y., Yang, Y., & Zhang, C. (2019). Assessing the performance of CMIP5 global climate models for simulating future precipitation change in the Tibetan Plateau. *Water*, 11(9), 1771. <https://doi.org/10.3390/w11091771>
- Joswiak, D. R., Yao, T., Wu, G., Tian, L., & Xu, B. (2013). Ice-core evidence of westerly and monsoon moisture contributions in the central Tibetan Plateau. *Journal of Glaciology*, 59(213), 56–66. <https://doi.org/10.3189/2013jog12j035>
- Kalnay, E., Kanamitsu, M., Kistler, R., Collins, W., Deaven, D., Gandin, L., et al. (1996). The NCEP/NCAR 40-year reanalysis project. *Bulletin of the American Meteorological Society*, 77(3), 437–472. [https://doi.org/10.1175/1520-0477\(1996\)077<0437:tnyrp>2.0.co;2](https://doi.org/10.1175/1520-0477(1996)077<0437:tnyrp>2.0.co;2)
- Kaspari, S., Mayewski, P., Kang, S., Sneed, S., Hou, S., Hooke, R., et al. (2007). Reduction in northward incursions of the South Asian monsoon since~1400 AD inferred from a Mt. Everest ice core. *Geophysical Research Letters*, 34(16), L16701. <https://doi.org/10.1029/2007gl030440>
- Klein, S. A., & Hall, A. (2015). Emergent constraints for cloud feedbacks. *Current Climate Change Reports*, 1(4), 276–287. <https://doi.org/10.1007/s40641-015-0027-1>
- Kong, Y., Wang, K., Li, J., & Pang, Z. (2019). Stable isotopes of precipitation in China: A consideration of moisture sources. *Water*, 11(6), 1239. <https://doi.org/10.3390/w11061239>
- Kumar, S., Hazra, A., & Goswami, B. N. (2014). Role of interaction between dynamics, thermodynamics and cloud microphysics on summer monsoon precipitating clouds over the Myanmar Coast and the Western Ghats. *Climate Dynamics*, 43(3), 911–924. <https://doi.org/10.1007/s00382-013-1909-3>
- Kurita, N., & Yamada, H. (2008). The role of local moisture recycling evaluated using stable isotope data from over the middle of the Tibetan plateau during the monsoon season. *Journal of Hydrometeorology*, 9(4), 760–775. <https://doi.org/10.1175/2007jhm945.1>
- Kurita, N., Noone, D., Risi, C., Schmidt, G. A., Yamada, H., & Yoneyama, K. (2011). Intraseasonal isotopic variation associated with the Madden-Julian oscillation. *Journal of Geophysical Research*, 116, D24. <https://doi.org/10.1029/2010jd015209>
- Lawrence, J. R., Gedzelman, S. D., Dexheimer, D., Cho, H. K., Carrie, G. D., Gasparini, R., et al. (2004). Stable isotopic composition of water vapor in the tropics. *Journal of Geophysical Research*, 109(D6). <https://doi.org/10.1029/2003jd004046>
- Lee, J. E., Fung, I., De Paolo, D. J., & Henning, C. C. (2007). Analysis of the global distribution of water isotopes using the NCAR atmospheric general circulation model. *Journal of Geophysical Research*, 112, D16. <https://doi.org/10.1029/2006jd007657>
- Lee, J. E., Fung, I., Risi, C., Worden, J., Scheepmaker, R., & Frankenberg, C. (2012). Asian monsoon hydrology from LMDZ GCM and two satellite measurements (TES and SCIAMACHY) of water vapor isotopes: Implications for speleothem data interpretation. *Journal of Geophysical Research*, 117(D15), D15112. <https://doi.org/10.1029/2011jd017133>
- LeGrande, A. N., & Schmidt, G. A. (2009). Sources of Holocene variability of oxygen isotopes in paleoclimate archives. *Climate of the Past*, 5(3), 441–455. <https://doi.org/10.5194/cp-5-441-2009>
- Liu, Z., Wen, X., Brady, E. C., Otto-Bliesner, B., Yu, G., Lu, H., et al. (2014). Chinese cave records and the East Asia summer monsoon. *Quaternary Science Reviews*, 83, 115–128. <https://doi.org/10.1016/j.quascirev.2013.10.021>
- Mapes, B., & Neale, R. (2011). Parameterizing convective organization to escape the entrainment dilemma. *Journal of Advances in Modeling Earth Systems*, 3(2). <https://doi.org/10.1029/2011ms000042>
- Maupin, C. R., Roark, E. B., Thirumalai, K., Shen, C. C., Schumacher, C., Kampen-Lewis, V., et al. (2021). Abrupt Southern Great Plains thunderstorm shifts linked to glacial climate variability. *Nature Geoscience*, 14(6), 396–401. <https://doi.org/10.1038/s41561-021-00729-w>
- Midhun, M., & Ramesh, R. (2016). Validation of δ¹⁸O as a proxy for past monsoon rain by multi-GCM simulations. *Climate Dynamics*, 46(5–6), 1371–1385. <https://doi.org/10.1007/s00382-015-2652-8>
- Midhun, M., Lekshmy, P. R., Ramesh, R., Yoshimura, K., Sandeep, K. K., Kumar, S., et al. (2018). The effect of monsoon circulation on the stable isotopic composition of rainfall. *Journal of Geophysical Research: Atmospheres*, 123(10), 5205–5221. <https://doi.org/10.1029/2017jd027427>
- Mölg, T., Maussion, F., & Scherer, D. (2014). Mid-latitude westerlies as a driver of glacier variability in monsoonal High Asia. *Nature Climate Change*, 4(1), 68–79. <https://doi.org/10.1038/nclimate2055>
- Münch, T., & Laepple, T. (2018). What climate signal is contained in decadal-to centennial-scale isotope variations from Antarctic ice cores? *Climate of the Past*, 14(12), 2053–2070. <https://doi.org/10.5194/cp-14-2053-2018>
- Nimya, S. S., Sengupta, S., Parekh, A., Bhattacharya, S. K., & Pradhan, R. (2022). Region-specific performances of isotope enabled general circulation models for Indian summer monsoon and the factors controlling isotope biases. *Climate Dynamics*, 59(11–12), 1–21. <https://doi.org/10.1007/s00382-022-06286-1>
- Noone, D. (2012). Pairing measurements of the water vapor isotope ratio with humidity to deduce atmospheric moistening and dehydration in the tropical midtroposphere. *Journal of Climate*, 25(13), 4476–4494. <https://doi.org/10.1175/jcli-d-11-00582.1>
- Pai, D. S., Sridhar, L., Badwaik, M. R., & Rajeevan, M. (2015). Analysis of the daily rainfall events over India using a new long period (1901–2010) high resolution (0.25×0.25) gridded rainfall data set. *Climate Dynamics*, 45(3), 755–776. <https://doi.org/10.1007/s00382-014-2307-1>
- Randall, D., Branson, M., Wang, M., Ghan, S., Craig, C., Gettelman, A., & Edwards, J. (2013). A community atmosphere model with superparameterized clouds. *Eos, Transactions American Geophysical Union*, 94(25), 221–222. <https://doi.org/10.1002/2013eo250001>
- Rio, C., Del Genio, A. D., & Hourdin, F. (2019). Ongoing breakthroughs in convective parameterization. *Current Climate Change Reports*, 5(2), 95–111. <https://doi.org/10.1007/s40641-019-00127-w>
- Risi, C., Bony, S., Vimeux, F., & Jouzel, J. (2010). Water-stable isotopes in the LMDZ4 general circulation model: Model evaluation for present-day and past climates and applications to climatic interpretations of tropical isotopic records. *Journal of Geophysical Research*, 115(D12), D12118. <https://doi.org/10.1029/2009jd013255>
- Risi, C., Bony, S., Vimeux, F., Descroix, L., Ibrahim, B., Lebreton, E., et al. (2008). What controls the isotopic composition of the African monsoon precipitation? Insights from event-based precipitation collected during the 2006 AMMA field campaign. *Geophysical Research Letters*, 35(24), L24808. <https://doi.org/10.1029/2008gl035920>
- Risi, C., Muller, C., & Blossey, P. (2021). Rain evaporation, snow melt, and entrainment at the heart of water vapor isotopic variations in the tropical troposphere, according to large-eddy simulations and a two-column model. *Journal of Advances in Modeling Earth Systems*, 13(4), e2020MS002381. <https://doi.org/10.1029/2020ms002381>
- Risi, C., Noone, D., Frankenberg, C., & Worden, J. (2013). Role of continental recycling in intraseasonal variations of continental moisture as deduced from model simulations and water vapor isotopic measurements. *Water Resources Research*, 49(7), 4136–4156. <https://doi.org/10.1002/wrcr.20312>
- Risi, C., Noone, D., Worden, J., Frankenberg, C., Stiller, G., Kiefer, M., et al. (2012a). Process-evaluation of tropospheric humidity simulated by general circulation models using water vapor isotopologues: 1. Comparison between models and observations. *Journal of Geophysical Research*, 117(D5). <https://doi.org/10.1029/2011jd016621>

- Risi, C., Noone, D., Worden, J., Frankenberg, C., Stiller, G., Kiefer, M., et al. (2012b). Process-evaluation of tropospheric humidity simulated by general circulation models using water vapor isotopic observations: 2. Using isotopic diagnostics to understand the mid and upper tropospheric moist bias in the tropics and subtropics. *Journal of Geophysical Research*, *117*(D5). <https://doi.org/10.1029/2011jd016623>
- Rozanski, K., Araguás-Araguás, L., & Gonfiantini, R. (1993). Isotopic patterns in modern global precipitation. *GMS*, *78*, 1–36.
- Schmidt, G. A., Hoffmann, G., Shindell, D. T., & Hu, Y. (2005). Modeling atmospheric stable water isotopes and the potential for constraining cloud processes and stratosphere-troposphere water exchange. *Journal of Geophysical Research*, *110*(D21), D21314. <https://doi.org/10.1029/2005jd005790>
- Schmidt, G. A., LeGrande, A. N., & Hoffmann, G. (2007). Water isotope expressions of intrinsic and forced variability in a coupled ocean-atmosphere model. *Journal of Geophysical Research*, *112*(D10). <https://doi.org/10.1029/2006jd007781>
- Schumacher, C., Houze, R. A., Jr., & Kraucunas, I. (2004). The tropical dynamical response to latent heating estimates derived from the TRMM precipitation radar. *Journal of the Atmospheric Sciences*, *61*(12), 1341–1358. [https://doi.org/10.1175/1520-0469\(2004\)061<1341:tdrtl>2.0.co;2](https://doi.org/10.1175/1520-0469(2004)061<1341:tdrtl>2.0.co;2)
- Sengupta, S., & Sarkar, A. (2006). Stable isotope evidence of dual (Arabian Sea and Bay of Bengal) vapour sources in monsoonal precipitation over north India. *Earth and Planetary Science Letters*, *250*(3–4), 511–521. <https://doi.org/10.1016/j.epsl.2006.08.011>
- Sengupta, S., Bhattacharya, S. K., Parekh, A., Nimya, S. S., Yoshimura, K., & Sarkar, A. (2020). Signatures of monsoon intra-seasonal oscillation and stratiform process in rain isotope variability in northern Bay of Bengal and their simulation by isotope enabled general circulation model. *Climate Dynamics*, *55*(5), 1649–1663. <https://doi.org/10.1007/s00382-020-05344-w>
- Shen, H., & Poulsen, C. J. (2019). Precipitation $\delta^{18}\text{O}$ on the Himalaya–Tibet orogeny and its relationship to surface elevation. *Climate of the Past*, *15*(1), 169–187. <https://doi.org/10.5194/cp-15-169-2019>
- Shi, X., Risi, C., Pu, T., Lacour, J. L., Kong, Y., Wang, K., et al. (2020). Variability of isotope composition of precipitation in the Southeastern Tibetan Plateau from the synoptic to seasonal time scale. *Journal of Geophysical Research: Atmospheres*, *125*(6), e2019JD031751. <https://doi.org/10.1029/2019jd031751>
- Sime, L. C., Wolff, E. W., Oliver, K. I. C., & Tindall, J. C. (2009). Evidence for warmer interglacials in East Antarctic ice cores. *Nature*, *462*(7271), 342–345. <https://doi.org/10.1038/nature08564>
- Sperber, K. R., Annamalai, H., Kang, I. S., Kitoh, A., Moise, A., Turner, A., et al. (2013). The Asian summer monsoon: An intercomparison of CMIP5 vs. CMIP3 simulations of the late 20th century. *Climate Dynamics*, *41*(9–10), 2711–2744. <https://doi.org/10.1007/s00382-012-1607-6>
- Stevens, B., & Bony, S. (2013). What are climate models missing? *Science*, *340*(6136), 1053–1054. <https://doi.org/10.1126/science.1237554>
- Su, F., Duan, X., Chen, D., Hao, Z., & Cuo, L. (2013). Evaluation of the global climate models in the CMIP5 over the Tibetan Plateau. *Journal of Climate*, *26*(10), 3187–3208. <https://doi.org/10.1175/jcli-d-12-00321.1>
- Tabor, C. R., Otto-Bliesner, B. L., Brady, E. C., Nusbaumer, J., Zhu, J., Erb, M. P., et al. (2018). Interpreting precession-driven $\delta^{18}\text{O}$ variability in the South Asian monsoon region. *Journal of Geophysical Research: Atmospheres*, *123*(11), 5927–5946. <https://doi.org/10.1029/2018jd028424>
- Thompson, L. G., Yao, T., Mosley-Thompson, E., Davis, M., Henderson, K., & Lin, P.-N. (2000). A high-resolution millennial record of the South Asian monsoon from Himalayan ice cores. *Science*, *289*(5486), 1916–1919. <https://doi.org/10.1126/science.289.5486.1916>
- Thompson, L. O., Yao, T., Davis, M. E., Henderson, K. A., Mosley-Thompson, E., Lin, P. N., et al. (1997). Tropical climate instability: The last glacial cycle from a Qinghai-Tibetan ice core. *Science*, *276*(5320), 1821–1825. <https://doi.org/10.1126/science.276.5320.1821>
- Tian, L., Ma, L., Yu, W., Liu, Z., Yin, C., Zhao, Z., et al. (2008). Seasonal variations of stable isotope in precipitation and moisture transport at Yushu, eastern Tibetan Plateau. *Science in China - Series D: Earth Sciences*, *51*(8), 1121–1128. <https://doi.org/10.1007/s11430-008-0089-1>
- Tian, L., Masson-Delmotte, V., Stievenard, M., Yao, T., & Jouzel, J. (2001). Tibetan Plateau summer monsoon northward extent revealed by measurements of water stable isotopes. *Journal of Geophysical Research*, *106*(D22), 28081–28088. <https://doi.org/10.1029/2001jd900186>
- Tian, L., Yao, T., MacClune, K., White, J. W. C., Schilla, A., Vaughn, B., et al. (2007). Stable isotopic variations in west China: A consideration of moisture sources. *Journal of Geophysical Research*, *112*(D10). <https://doi.org/10.1029/2006jd007718>
- Tindall, J. C., Valdes, P. J., & Sime, L. C. (2009). Stable water isotopes in HadCM3: Isotopic signature of El Niño–southern oscillation and the tropical amount effect. *Journal of Geophysical Research*, *114*(D4), D04111. <https://doi.org/10.1029/2008jd010825>
- Tremoy, G., Vimeux, F., Soumana, S., Souley, I., Risi, C., Favreau, G., & Oï, M. (2014). Clustering mesoscale convective systems with laser-based water vapor $\delta^{18}\text{O}$ monitoring in Niamey (Niger). *Journal of Geophysical Research: Atmospheres*, *119*(9), 5079–5103. <https://doi.org/10.1002/2013jd020968>
- Vuille, M., Bradley, R. S., Werner, M., Healy, R., & Keimig, F. (2003). Climate and dynamics (ACL)-ACL1-Modeling $\delta^{18}\text{O}$ in precipitation over the tropical Americas: 1. Interannual variability and climatic controls. *Journal of Geophysical Research-Part D-Atmospheres*, *108*(6), 2001JD002038. <https://doi.org/10.1029/2001jd002038>
- Wang, Y. J., Cheng, H., Edwards, R. L., An, Z. S., Wu, J. Y., Shen, C. C., & Dorale, J. A. (2001). A high-resolution absolute-dated late Pleistocene monsoon record from Hulu Cave, China. *Science*, *294*(5550), 2345–2348. <https://doi.org/10.1126/science.1064618>
- Wang, Y., Cheng, H., Edwards, R. L., Kong, X., Shao, X., Chen, S., et al. (2008). Millennial- and orbital-scale changes in the East Asian monsoon over the past 224,000 years. *Nature*, *451*(7182), 1090–1093. <https://doi.org/10.1038/nature06692>
- Webb, M. J., Lock, A. P., Bretherton, C. S., Bony, S., Cole, J. N., Idelkadi, A., et al. (2015). The impact of parametrized convection on cloud feedback. *Philosophical Transactions of the Royal Society A: Mathematical, Physical and Engineering Sciences*, *373*(2054), 20140414. <https://doi.org/10.1098/rsta.2014.0414>
- Werner, M., Langebroek, P. M., Carlsen, T., Herold, M., & Lohmann, G. (2011). Stable water isotopes in the ECHAM5 general circulation model: Toward high-resolution isotope modeling on a global scale. *Journal of Geophysical Research*, *116*(D15), D15109. <https://doi.org/10.1029/2011jd015681>
- Worden, J., Bowman, K., Noone, D., Beer, R., Clough, S., Eldering, A., et al. (2006). Tropospheric Emission Spectrometer observations of the tropospheric HDO/H₂O ratio: Estimation approach and characterization. *Journal of Geophysical Research*, *111*(D16), D16309. <https://doi.org/10.1029/2005jd006606>
- Worden, J., Noone, D., & Bowman, K. (2007). Importance of rain evaporation and continental convection in the tropical water cycle. *Nature*, *445*(7127), 528–532. <https://doi.org/10.1038/nature05508>
- Wu, G., & Zhang, Y. (1998). Tibetan Plateau forcing and the timing of the monsoon onset over South Asia and the South China Sea. *Monthly Weather Review*, *126*(4), 913–927. [https://doi.org/10.1175/1520-0493\(1998\)126<0913:tpf>2.0.co;2](https://doi.org/10.1175/1520-0493(1998)126<0913:tpf>2.0.co;2)
- Wu, H., Li, X. Y., Zhang, J., Li, J., Liu, J., Tian, L., & Fu, C. (2019). Stable isotopes of atmospheric water vapour and precipitation in the northeast Qinghai-Tibetan Plateau. *Hydrological Processes*, *33*(23), 2997–3009. <https://doi.org/10.1002/hyp.13541>
- Wu, H., Zhang, X., Xiaoyan, L., Li, G., & Huang, Y. (2015). Seasonal variations of deuterium and oxygen-18 isotopes and their response to moisture source for precipitation events in the subtropical monsoon region. *Hydrological Processes*, *29*(1), 90–102. <https://doi.org/10.1002/hyp.10132>
- Yanai, M., & Wu, G. X. (2006). Effects of the Tibetan plateau. In *The asian monsoon* (pp. 513–549). Springer.

- Yanai, M., Esbensen, S., & Chu, J. H. (1973). Determination of bulk properties of tropical cloud clusters from large-scale heat and moisture budgets. *Journal of the Atmospheric Sciences*, *30*(4), 611–627. [https://doi.org/10.1175/1520-0469\(1973\)030<0611:dobpot>2.0.co;2](https://doi.org/10.1175/1520-0469(1973)030<0611:dobpot>2.0.co;2)
- Yang, B., Braeuning, A., Yao, T., & Davis, M. E. (2007). Correlation between the oxygen isotope record from Dasuopu ice core and the Asian Southwest Monsoon during the last millennium. *Quaternary Science Reviews*, *26*(13–14), 1810–1817. <https://doi.org/10.1016/j.quascirev.2007.03.003>
- Yang, K., Wu, H., Qin, J., Lin, C., Tang, W., & Chen, Y. (2014). Recent climate changes over the Tibetan plateau and their impacts on energy and water cycle: A review. *Global and Planetary Change*, *112*, 79–91. <https://doi.org/10.1016/j.gloplacha.2013.12.001>
- Yang, X. X., Davis, M. E., Acharya, S., & Yao, T. D. (2018). Asian monsoon variations revealed from stable isotopes in precipitation. *Climate Dynamics*, *51*(5–6), 2267–2283. <https://doi.org/10.1007/s00382-017-4011-4>
- Yang, X., & Yao, T. (2020). Seasonality of moisture supplies to precipitation over the third Pole: A stable water isotopic perspective. *Scientific Reports*, *10*(1), 1–12. <https://doi.org/10.1038/s41598-020-71949-0>
- Yang, X., Yao, T., Yang, W., Xu, B., He, Y., & Qu, D. (2012). Isotopic signal of earlier summer monsoon onset in the Bay of Bengal. *Journal of Climate*, *25*(7), 2509–2516. <https://doi.org/10.1175/jcli-d-11-00180.1>
- Yao, T., Masson-Delmotte, V., Gao, J., Yu, W., Yang, X., Risi, C., et al. (2013). A review of climatic controls on $\delta^{18}\text{O}$ in precipitation over the Tibetan Plateau: Observations and simulations. *Reviews of Geophysics*, *51*(4), 525–548. <https://doi.org/10.1002/rog.20023>
- Yao, T., Shi, Y., & Thompson, L. G. (1997a). High resolution record of paleoclimate since the Little Ice Age from the Tibetan ice cores. *Quaternary International*, *37*, 19–23. [https://doi.org/10.1016/1040-6182\(96\)00006-7](https://doi.org/10.1016/1040-6182(96)00006-7)
- Yao, T., Thompson, L. G., Mosley-Thompson, E., Yang, Z. H., Zhang, X. P., & Lin, P. N. (1996). Climatological significance of $\delta^{18}\text{O}$ in north Tibetan ice cores. *Journal of Geophysical Research*, *101*(D23), 29531–29537. <https://doi.org/10.1029/96jd02683>
- Yao, T., Thompson, L. G., Shi, Y., Qin, D., Jiao, K., Yang, Z., et al. (1997b). Climate variation since the last interglaciation recorded in the Guliya ice core. *Science in China - Series D: Earth Sciences*, *40*(6), 662–668. <https://doi.org/10.1007/bf02877697>
- Yao, T., Thompson, L., Yang, W., Yu, W., Gao, Y., Guo, X., et al. (2012). Different glacier status with atmospheric circulations in Tibetan Plateau and surroundings. *Nature Climate Change*, *2*(9), 663–667. <https://doi.org/10.1038/nclimate1580>
- Yoshimura, K., Kanamitsu, M., Noone, D., & Oki, T. (2008). Historical isotope simulation using reanalysis atmospheric data. *Journal of Geophysical Research*, *113*(D19), D19108. <https://doi.org/10.1029/2008jd010074>
- Yu, R., Li, J., Zhang, Y., & Chen, H. (2015). Improvement of rainfall simulation on the steep edge of the Tibetan Plateau by using a finite-difference transport scheme in CAM5. *Climate Dynamics*, *45*(9–10), 2937–2948. <https://doi.org/10.1007/s00382-015-2515-3>
- Yu, W., Tian, L., Risi, C., Yao, T., Ma, Y., Zhao, H., et al. (2016). $\delta^{18}\text{O}$ records in water vapor and an ice core from the eastern Pamir Plateau: Implications for paleoclimate reconstructions. *Earth and Planetary Science Letters*, *456*, 146–156. <https://doi.org/10.1016/j.epsl.2016.10.001>
- Yu, W., Yao, T., Lewis, S., Tian, L., Ma, Y., Xu, B., & Qu, D. (2014). Stable oxygen isotope differences between the areas to the north and south of Qinling Mountains in China reveal different moisture sources. *International Journal of Climatology*, *34*(6), 1760–1772. <https://doi.org/10.1002/joc.3799>
- Yu, W., Yao, T., Thompson, L. G., Jouzel, J., Zhao, H., Xu, B., et al. (2020). Temperature signals of ice core and speleothem isotopic records from Asian monsoon region as indicated by precipitation $\delta^{18}\text{O}$. *Earth and Planetary Science Letters*, *554*, 116665. <https://doi.org/10.1016/j.epsl.2020.116665>
- Yu, W., Yao, T., Tian, L., Li, Z., Sun, W., & Wang, Y. (2006). Relationships between $\delta^{18}\text{O}$ in summer precipitation and temperature and moisture trajectories at Muztagata, Western China. *Science in China, Series A D*, *49*(1), 27–35. <https://doi.org/10.1007/s11430-004-5097-1>
- Yu, W., Yao, T., Tian, L., Ma, Y., Ichiyangi, K., Wang, Y., & Sun, W. (2008). Relationships between $\delta^{18}\text{O}$ in precipitation and air temperature and moisture origin on a south-north transect of the Tibetan Plateau. *Atmospheric Research*, *87*(2), 158–169. <https://doi.org/10.1016/j.atmosres.2007.08.004>
- Yu, W., Yao, T., Tian, L., Ma, Y., Wen, R., Devkota, L. P., et al. (2016). Short-term variability in the dates of the Indian monsoon onset and retreat on the southern and northern slopes of the central Himalayas as determined by precipitation stable isotopes. *Climate Dynamics*, *47*(1–2), 159–172. <https://doi.org/10.1007/s00382-015-2829-1>
- Zhang, X. P., Sun, Z. A., Guan, H. D., Zhang, X. Z., Wu, H. W., & Huang, Y. M. (2011). GCM simulation of stable water isotopes in water cycle and intercomparisons over East Asia. *Journal of Glaciology and Geocryology*, *33*(6), 1274–1285.
- Zhao, H., Xu, B., Li, Z., Wang, M., Li, J., & Zhang, X. (2017). Abundant climatic information in water stable isotope record from a maritime glacier on southeastern Tibetan Plateau. *Climate Dynamics*, *48*(3–4), 1161–1171. <https://doi.org/10.1007/s00382-016-3133-4>
- Zhu, Y. Y., & Yang, S. (2020). Evaluation of CMIP6 for historical temperature and precipitation over the Tibetan Plateau and its comparison with CMIP5. *Advances in Climate Change Research*, *11*(3), 239–251. <https://doi.org/10.1016/j.accre.2020.08.001>

References From the Supporting Information

- Bartlein, P. J., Harrison, S. P., Brewer, S., Connor, S., Davis, B. A. S., Gajewski, K., et al. (2011). Pollen-based continental climate reconstructions at 6 and 21 ka: A global synthesis. *Climate Dynamics*, *37*(3), 775–802. <https://doi.org/10.1007/s00382-010-0904-1>
- Brierley, C. M., Zhao, A., Harrison, S. P., Braconnot, P., Williams, C. J., Thornalley, D. J., et al. (2020). Large-scale features and evaluation of the PMIP4-CMIP6 midHolocene simulations. *Climate of the Past*, *16*(5), 1847–1872. <https://doi.org/10.5194/cp-16-1847-2020>
- Caley, T., & Roche, D. M. (2013). $\delta^{18}\text{O}$ water isotope in the iLOVECLIM model (version 1.0)—Part 3: A palaeo-perspective based on present-day data—model comparison for oxygen stable isotopes in carbonates. *Geoscientific Model Development*, *6*(5), 1505–1516. <https://doi.org/10.5194/gmd-6-1505-2013>
- Lin, Y., Ramstein, G., Wu, H., Rani, R., Braconnot, P., Kageyama, M., et al. (2019). Mid-holocene climate change over China: Model–data discrepancy. *Climate of the Past*, *15*(4), 1223–1249. <https://doi.org/10.5194/cp-15-1223-2019>
- Sherwood, S. C., Bony, S., & Dufresne, J. L. (2014). Spread in model climate sensitivity traced to atmospheric convective mixing. *Nature*, *505*(7481), 37–42. <https://doi.org/10.1038/nature12829>
- Vuille, M., & Werner, M. (2004). *Stable isotopes in precipitation and the south American summer monsoon-observations and model results* (pp. C43D–C08). AGUFM.